

1 **Sedimentary organic matter signature hints at the phytoplankton-driven Biological**
2 **Carbon Pump in the Central Arabian Sea**

3 **Medhavi Pandey^{1,2}, Haimanti Biswas^{1,2*}, Daniel Birgel³, Nicole Burdanowitz³, Birgit**
4 **Gaye³**

5 ¹CSIR National Institute of Oceanography, Biological Oceanography Division, Dona Paula, Goa
6 403004. India.

7 ²Academy of Scientific and Innovative Research (AcSIR), Ghaziabad-201002, India.

8 ³Institute for Geology, Center for Earth System Research and Sustainability (CEN), Universität
9 Hamburg, Bundesstraße55, 20146, Hamburg, Germany.

10 *Corresponding Author's email: haimanti.biswas.nio@gmail.com; haimanti.biswas@nio.org

11 **Abstract**

12 The Central Arabian Sea, a unique tropical basin is profoundly impacted by monsoon wind
13 reversal affecting its surface circulation and biogeochemistry. Phytoplankton blooms
14 associated with high biological productivity and particle flux occur in the northern part of the
15 central Arabian Sea due to summer monsoon-induced open ocean upwelling and winter
16 convection. The core Oxygen Minimum Zone (OMZ) at intermediate water depths is another
17 important feature of the north-central Arabian Sea and fades southward. In this study, we
18 attempt to interlink how these factors collectively impact phytodetrital export to the sediment.
19 Short sediment core top (1 cm) samples representing the recent particle flux signatures were
20 analyzed from 5 locations (21° to 11° N; 64° E) in the central Arabian Sea. Previously, we used
21 core top (0-0.5 cm) samples and observed a trend between diatom frustule abundance and
22 diversity with bulk sedimentary parameters indicating a spatial variability in phytodetrital
23 export to the sediment. To verify this observation further, lipid biomarkers of key
24 phytoplankton groups and a sea surface temperature (SST) proxy have been analyzed in
25 addition to diatom frustules. The C₃₇ alkenone-based SST proxy indicated cooler SST (27.6 ±
26 0.25 °C) in the north (21–15° N) mostly due to upwelling (summer) and convective mixing
27 (winter). Warmer SSTs (+0.4 °C) are measured in the south, which usually remains nutrient-
28 poor. This trend was consistent with satellite-derived average SST values (2017–2020). Lipid
29 biomarker analysis suggests that dinoflagellates were likely to be the highest contributor as
30 indicated by dinosterol and its degradative product dinostanol, followed by brassicasterol and
31 C₃₇ alkenone, likely representing diatoms and coccolithophores, respectively. The north, which
32 largely experiences periodic phytoplankton blooms and is influenced by the thick OMZ,
33 revealed the highest contents of organic matter, diatom frustules (diversity and abundance),
34 dominated by large thickly silicified cells (e.g. *Coscinodiscus* and *Rhizosolenia*), and
35 phytoplankton lipid biomarkers, as well as lower contents of zooplankton biomarkers
36 (cholesterol and cholestanol). In contrast, relatively smaller chain-forming centric (e.g.
37 *Thalassiosira*) and pennate (e.g. *Pseudo-nitzschia*, *Nitzschia*, *Thalassionema*) diatom frustules
38 along with lower phytoplankton lipid biomarker contents were found in the south where
39 zooplankton biomarkers and silicious radiolarians were more abundant. The possible impacts
40 of OMZ on particle flux related to the phytoplankton community, including zooplankton
41 grazing and other factors have been discussed.

42
43 **Keywords: Phytodetritus; North Indian Ocean; Monsoon; Biomarkers; Brassicasterol;**
44 **Dinosterol**

48 1. Introduction

49 Marine phytoplankton modulate the global carbon cycle by fixing almost 48 Gt C annually
50 (Singh and Ahluwalia, 2013) which corresponds to 50% of the global primary production
51 (Field et al., 1998; Behrenfeld et al., 2006). This amount of organic matter produced within the
52 euphotic layers, where more than 1% of sunlight arrives, supports the entire marine food chain
53 including the benthic population. Nearly 10% of this organic matter (large and dense
54 phytodetritus) sinks to the upper mesopelagic ocean and gets further fragmented by
55 zooplankton and microbially remineralized on its descent into the deep ocean. Only 1–3% of
56 this phytodetritus can reach the seafloor below 1000 m water depth (Iversen, 2023) and can be
57 stored for hundreds to millions of years (Buesseler, 1998), and is called sequestration flux. This
58 way of trapping carbon from the atmosphere to the ocean interior mediated by phytoplankton
59 is called the Biological Carbon Pump (BCP) (Volk and Hoffert, 1985; Le Moigne, 2019;
60 Iversen, 2023 and references therein). However, the organic matter in the surface sediment can
61 be further modified biogeochemically. The strength of BCP is governed by many factors, such
62 as heterotrophic remineralization of organic matter, dissolved oxygen (DO) levels,
63 temperature, phytoplankton community composition, cell size, and zooplankton activity
64 (Marsay et al., 2015; Keil et al., 2016; Cavan et al., 2017; Engel et al., 2017; Iversen, 2023).
65 Out of multiple factors controlling the efficacy of the BCP, phytoplankton community
66 composition (that controls organic matter stoichiometry), zooplankton grazing (Cavan et al.,
67 2017), and mid-water oxygen concentrations (Keil et al., 2016) are crucial factors. Thus,
68 understanding the functioning of the marine BCP in productive marine ecosystems needs
69 attention, particularly in the context of changing climate (Iversen, 2023).

70 Diatom frustules, dinoflagellate cysts, and lipid biomarkers (e.g. sterols, alkenones) preserved
71 in sediments could be potential proxies for the reconstruction of productivity and organic
72 matter transport from the surface to the deep sea floor (Liu et al., 2013; Hu et al., 2020; Xiong
73 et al., 2020 and references therein). The responses of phytoplankton to changing climate as
74 well as other environmental variables can be retrieved from the sediments and may help predict
75 future primary production, community shifts in marine ecosystems, and the ocean's role as a
76 carbon sink. Generally, the siliceous frustules of diatoms are more resistant to grazing and
77 degradation and can be better preserved in sediments compared to other phytoplankton groups.
78 Sedimentary organic carbon, nitrogen, and their ratios, diatom frustules, and lipid biomarkers
79 (e.g. sterols and alkenones) are used to reconstruct past phytoplankton community shifts and
80 temperatures (Schubert et al., 1998; Liu et al., 2013; Rodríguez-Miret et al., 2023). The lipid
81 biomarkers of phytodetritus from the surface sediments can also provide valuable information
82 about the surface processes controlling phytoplankton growth (Xiong et al., 2020). For example
83 in a study by Peng et al. (2023), phytoplankton community shift was evident from lipid
84 biomarkers in the sediment core samples from the East China Sea. In a few studies, major
85 phytoplankton-derived lipid biomarkers like dinosterol, brassicasterol, and alkenone were also
86 used to correlate their contents with palaeoproductivity and associated changes of the sea ice
87 levels in the Arctic Ocean (Müller et al., 2011, and references therein).

88 The Arabian Sea in the northwestern part of the Indian Ocean is a unique marine province with
89 several characteristic features, for instance, the direct influence of monsoon winds on
90 oceanographic and biogeochemical processes, high productivity (McCreary et al., 2009), and
91 one of the thickest (200–1200 m) oxygen minimum zones (OMZ) in modern oceans (Banse et
92 al., 2014). The entire area experiences periodic reversals of monsoon winds and surface
93 circulation. During the summer (SW) monsoon, a low-level atmospheric jet (the Findlater Jet;
94 Findlater, 1971) blows parallel to the Omani and Somalia coasts, generating coastal and open

95 ocean upwelling in its northern part. Subsequently, due to natural nutrient enrichment,
96 phytoplankton blooms develop (Banse, 1987; Bhattathiri et al., 1996; Prasanna Kumar et al.,
97 2000). In the winter (NE) monsoon, winds and surface circulation reverse and in the northern
98 Arabian Sea, the cooling and densification of surface water leads to convective mixing
99 (Prasannakumar et al., 2001) that also fuels high phytoplankton growth (Madhupratap et al.,
100 1996).

101
102 In the Arabian Sea, the magnitude of particle transfer to the deep sea floor is directly controlled
103 by the surface processes (Schulte et al., 1999, Rixen et al., 2019a). The central Arabian Sea
104 exhibits one of the highest particle flux rates ($1.3\text{--}3.3\text{ g C m}^{-2}\text{ year}^{-1}$) (Haake et al., 1993)
105 compared with other low-latitude seas (Rixen et al., 2019b). This is mostly associated with
106 enhanced biological productivity governed by summer monsoon-induced upwelling and winter
107 convection (Nair et al., 1989; Haake et al., 1993; Rixen et al., 2019a). Nevertheless, particle
108 flux could vary significantly (Nair et al., 1989; Prahl et al., 2000) during the intermonsoon and
109 premonsoon due to prevailing oligotrophy (Prasanna Kumar and Narvekar, 2005).

110
111 The impacts of atmospheric forcings and consequent biological response in the central Arabian
112 Sea have been studied thoroughly during the joint Global Ocean Flux Studies (JGOFS, from
113 1987 to 2003). The monsoon wind is the major controlling forcing of physical, chemical, and
114 biological processes in the surface ocean (McCearry et al., 2009) with high spatial and seasonal
115 variability (Prasanna Kumar and Narvekar, 2005). However, there has been no further
116 investigation in the last two decades, although ocean warming continued with high spatial
117 variability (Roxy et al., 2016; Sharma et al., 2023 and references therein). Our previous study
118 showed that diatom frustules retrieved from the surface sediments from the central (Pandey et
119 al., 2023) and the eastern (Pandey and Biswas, 2023) Arabian Sea could be an efficient
120 indicator of surface processes controlling euphotic phytoplankton communities. There are a
121 few studies from the Arabian Sea characterizing sedimentary organic carbon using
122 phytoplankton biomarkers (Schubert et al., 1998; Prahl et al., 2000; Schulte et al., 1999; 2000)
123 suggesting such proxies from the surface sediment may be quite useful to understand the spatial
124 variability in organic matter transport. Prahl et al. (2000) used phytoplankton biomarkers (e.g.
125 C_{37} -alkenones, dinosterol, β -sitosterol) from sediment trap samples as well as from the surface
126 sediments over a year from the central Arabian Sea ($15^{\circ}59'N$, $61^{\circ}30'E$) and showed the
127 seasonal variability of biological productivity. Nevertheless, the degradation of organic matter
128 in the water column could be quite high during their descent through the water column pointed
129 out by Wakeham et al. (2002) in their work on lipids from the water column of the western
130 Arabian Sea.

131
132 Importantly, the Arabian Sea is warming at a faster pace compared to other oceanic regions
133 (Roxy et al., 2016; Sharma et al., 2023), and how the phytoplankton-driven organic matter
134 transport may respond to that change is still poorly understood. Furthermore, recent modeling
135 studies (Vallivattathillam et al., 2023) as well as data from biogeochemical-Argo floats (Liu et
136 al. 2024) hinted at a possible thinning of the OMZ in the Arabian Sea that may substantially
137 impact organic matter degradation within the water column, specifically in the southern part
138 (Roxy et al., 2016). To fill this gap, we want to address three major questions in this study, 1)
139 Which phytoplankton group dominates the sedimentary organic matter in the various stations
140 of the transect from north to south? 2) Does high spatial variability in the phytoplankton
141 community composition driven by physical forcing also impact organic matter transport? 3)
142 What are the possible factors (hydrography, physicochemical conditions, and atmospheric
143 forcings) being responsible for such spatial variability in organic matter transport in this
144 region? To address these questions, we have measured key parameters from surface sediments

145 including lipid biomarkers, alkenone-based SST reconstruction, and diatom frustules combined
146 with a few recent in-situ observations on hydrography, biogeochemistry, and phytoplankton
147 community from the central Arabian Sea (Silori et al., 2021; Chowdhury et al., 2021; Pandey
148 et al., 2023; Chowdhury et al., 2024). In our previous study (Pandey et al., 2023) using the core
149 top (0–0.5 cm) samples we observed a trend between diatom frustules abundance and diversity
150 with sedimentary parameters and atmospheric forcings. In this study, lipid biomarkers of other
151 phytoplankton groups including diatoms are considered to understand their contribution to
152 organic matter flux. Further, a lipid biomarker as an SST proxy has also been studied to
153 correlate with atmospheric forcings.

154

155 **2. Methodology**

156 **2.1. Sample collection**

157

158 During cruise SSD–068 (Dec 2019 to Jan 2020) with *RV. Sindhu Sadhana* five short sediment
159 cores were obtained using a multicorer (Ocean Scientific International Limited Maxi Multi-
160 corer; core tubes 60 cm, outer diameter 11 cm and 10 cm inner diameter) along a transect from
161 11–21° N at 64° E (Fig. 1a). These short cores were collected at 21° N, 19° N, 15° N, 13° N,
162 and 11° N with varying water depths between 3000 m and 4500 m (Fig. 1a). The cores were
163 subsampled onboard immediately in 0.5 cm slices and were kept in pre-cleaned plastic
164 containers at 0–4 °C. The advantage of using a multicorer is better preservation of the topmost
165 parts of the sediment core compared to other devices like box or gravity coring (Barnett et al.,
166 1984). For this study, we used the top 1 cm (0–0.5 cm and 0.5–1 cm slices) of cores for all
167 related analyses. Note that the core top samples (0–0.5 cm) were analyzed for total inorganic
168 carbon (TIC), total organic carbon (TOC), total nitrogen (TN) as well as diatom frustules and
169 diversity including radiolarian abundance earlier by Pandey et al. (2023).

170

171 **2.2. Analytical method**

172 **2.2.1. Total inorganic carbon (TIC), total organic carbon (TOC), and total nitrogen (TN)** 173 **contents**

174 Sediment samples (0.5–1 cm) were dried at 60 °C overnight and ground using agate mortar and
175 pestle. Aliquots (10 mg) of sediment samples were taken in tin capsules. Total carbon (TC) and
176 TN were measured using a CHN Elemental analyzer (Euro Vector EA3000 series analyzer) at
177 the Central Analytical Facility of CSIR-National Institute of Oceanography, Goa, India) against
178 soil reference material NC soil standard (5g 338 40025 procured from Elemental Microanalysis
179 Ltd, UK, Soil Standard Clay OAS Cat No. B2051–Certificate No. 341506) used for carbon and
180 nitrogen with an analytical error of < 2%. The TIC contents were measured against the calcium
181 carbonate (CaCO₃) standard (Merck, Germany) in a coulometer attached to an acidification
182 module (Model CM5015 (UIC, USA). The accuracy and precision obtained from the results
183 were within ± 1.25%. TOC values were calculated by the difference between TC and TIC (TOC
184 =TC-TIC).

185 **2.2.2. Analysis of silica-bearing organisms from sediments**

186 The diatom frustules and other siliceous organisms from sediments (0.5–1 cm) were
187 enumerated following the method by Armbrrecht et al. (2018). The dried sediment subsamples
188 (50 mg) were taken in a 15 mL sterile polypropylene tube and were treated chemically with
189 10% HCl, 30% H₂O₂, and 0.01 N anhydrous sodium diphosphate (Na₄P₂O₇) for removing
190 carbonate, organic matter, and fine clay, respectively. After each chemical treatment, samples
191 were washed three times with 15 mL Milli-Q water. Finally, the residue remaining after the

192 last rinse and decantation was diluted with Milli-Q to 10 mL and was homogenized. A small
193 portion (1 mL) from this homogenized solution was analyzed under an inverted microscope
194 (Nikon Ti2) in a Sedgewick rafter counting chamber (Pyser, UK) at 400–600× magnification.
195 The classical identification keys by Tomas (1997), Desikachary (1989), and
196 <http://www.algaebase.org> were used. No centrifugation was used in this process to avoid the
197 breaking of frustules. Further, the diatoms more than half in size were considered complete
198 valves (Abrantes and Sancetta, 1985). The diatom abundance was expressed as valves g⁻¹ dry
199 sediment. Radiolarians were also enumerated along with diatom frustules and given as
200 individuals g⁻¹.

201 2.2.3 Biomarker analysis and SST proxy

202 Lipid biomarker analyses were carried out at the Institute for Geology, University of Hamburg,
203 Germany. About 11 g to 19 g of freeze-dried and ground samples were used to obtain total lipid
204 extracts (TLEs) by using an Accelerated Solvent Extractor (ASE200, DIONEX). Before
205 extraction, a known amount (10 ng μL⁻¹) of internal standards (14-heptacosanone,
206 nonadecanol, and dialkylglycerol ether-18 (DAGE-18)) were added to the samples. The ASE
207 extraction for each sample was carried out at 100°C and 1000 PSI for 5 minutes in 3 cycles by
208 using the solvent mixture dichloromethane: methanol (DCM: MeOH, 9:1). The TLEs were
209 then concentrated with rotary evaporation and were separated later into a hexane-soluble
210 (adding *n*-hexane) and hexane-insoluble (adding DCM) fraction via NaSO₄ column
211 chromatography. To separate the hexane-soluble fraction into a neutral- and acid fraction via
212 saponification (at 85°C for 2 hrs) a 5 % potassium hydroxide (KOH) in MeOH solution was
213 added to this fraction. Then, the neutral fractions were obtained by adding *n*-hexane to the
214 saponified fraction, vortexing, and pipetting the neutral fraction containing *n*-hexane layer into
215 a new vial. The neutral fractions were then separated into apolar-, ketone- (containing
216 alkenones), and polar fractions (containing sterols, stanols) by column chromatography packed
217 with deactivated silica gel (5 % H₂O, 60 μm mesh) using the solvents *n*-hexane, DCM, and
218 DCM: MeOH (1:1), respectively. We took 50% splits of the ketone- and polar fractions and
219 put them together, as some of the sterols and added standards for the sterol fraction were found
220 in the ketone fraction, too. For the derivatization of these fractions, a mixture of 200 μL
221 BSTFA: Pyridin (1:1) was added to the dried sample and heated at 80°C for 2 hrs followed by
222 drying under an N₂ environment.

223 To quantify the alkenones and sterols the samples were measured with a Thermo Scientific
224 Trace 1310 gas chromatography coupled to a flame ionization detector (GC-FID) equipped
225 with a Thermo Scientific TG-5MS column (30 m, 0.25 mm, 0.25 μm). H₂ as carrier gas was
226 used with a flow rate of 35 mL minute⁻¹ and the PTV injector started at 50°C ramped with
227 10°C/s to 325°C in a splitless mode. For the alkenones, the initial GC temperature was
228 programmed to 50°C (held 1 minute) and then ramped to a temperature of 230 °C with an
229 increased rate of 20 °C minute⁻¹, then increased at 4.5°C minute⁻¹ to 260 °C, and at 6 °C minute⁻¹
230 to 325 °C, which was held for 15 minutes. The peaks of alkenones were identified by
231 comparing the retention time for peaks of the samples with a known working sediment
232 standard. Quantification of the alkenones was done by using 14-heptacosane and
233 tetratriacontane with a known amount (10 ng μL⁻¹) as external standards. Repeated
234 measurements of the external standards yielded a quantification precision of 13 % (14-
235 heptacosanone) and 8 % (tetratriacontane). The alkenone saturation index was calculated using
236 the equation by Prahl et al. (1988):

$$237 U_{37}^{kl} = \frac{C_{37:2}}{C_{37:2} + C_{37:3}}$$

238 to convert the $U_{37}^{k'}$ index to SSTs we have used the core top calibration of Indian Ocean
239 sediments (Sonzogni et al., 1997):

$$240 \quad SST = \frac{U_{37}^{k'} - 0.043}{0.033}$$

241 For each sample, at least a duplicate measurement was conducted, which yielded an average
242 precision of 0.1 °C (1SD). Replicate extractions of a working standard sediment (n=2) and its
243 duplicate measurements where each replicate yielded an average precision of 0.5 °C (1 SD).

244 For the quantification of the sterols, the initial GC temperature was 50 °C (held for 3 minutes)
245 and then programmed to a final temperature of 325 °C (held for 20 minutes) with an increase
246 of 6 °C minute⁻¹. To quantify the sterols we used nonadecanol and DAGE-18 with a known
247 amount (10 ng µL) as external standards, with precision of 5.6 % and 4.9 %, respectively. To
248 identify the sterols the mass spectra of each sample were investigated using a Thermo Scientific
249 Trace GC Ultra coupled to a Thermo Scientific DSQ II mass spectrometer (GC-MS). He (2 mL
250 minute⁻¹ flow rate) was used as carrier gas. The initial GC temperature was 50 °C (held for 3
251 minutes) and ramped with 6 °C minute⁻¹ to 325 °C (held for 25 minutes). The mass spectra of
252 the compounds were then compared with published mass spectral data.

253 **2.2.4 Sea surface temperature (SST) and Chlorophyll *a* (Chl*a*) from satellite imagery**

254 The SST data was accessed from the climate reanalysis version 5 (ERA5) of the European
255 Centre for Medium-Range Weather Forecasts (ECMWF) (C3S, 2017). ERA5 covers the time
256 from 1979 to the present at a 0.25° × 0.25° grid. In this study, we used monthly mean of SST
257 data averaged for a period from 2017–2020 (downloaded from
258 <https://cds.climate.copernicus.eu/cdsapp#!/dataset/reanalysis-era5-single-levels?tab=form>.
259 Chl*a* values were derived from Aqua MODIS at a 4 km resolution. The average was calculated
260 from daily Chl*a* data during the period of 2017 Jan to 2020 Dec (downloaded from
261 <https://oceancolor.gsfc.nasa.gov/13/>).

262 **2.2.5 Statistical analysis**

263 The Shapiro-Wilk normality test and F test were used to check the normality and variance of
264 individual datasets, respectively. The statistical significance between differences for various
265 parameters was obtained using single-factor Analysis of Variance (ANOVA) in Microsoft
266 Excel 2019 at a 95% confidence level (probability $p < 0.05$). The correlations between the biotic
267 and environmental variables were derived using a linear multivariate model RDA (Redundancy
268 Analysis). The relationships between the key variables (biomarkers, frustules, radiolarian,
269 diatom community, TOC, TN, TOC: TN, TIC, and SST) are tested using the CANOCO version
270 4.5 software (Ter Braak and Šmilauer, 2002). In this test, cluster I contained biomarkers,
271 frustules, radiolarian, and diatom community, and cluster II included other variables (SST,
272 TOC, TN, TIC, TOC: TN).

273 **3. Results**

274 The sedimentary characteristics (TIC, TOC, TN), diatom frustule abundance, and diversity
275 including radiolarian abundance from this study (0.5–1 cm depth) and by Pandey et al. (2023,
276 core top 0–0.5 cm) are shown as average representing the top 1 cm of the surface sediment
277 (Table 1). Results of lipid biomarkers (0–0.5 and 0.5–1 cm) such as various phytosterols and
278 the summed C_{37:2} and C_{37:3} alkenones as well as $U_{37}^{k'}$ -derived sea surface temperatures (SSTs)
279 are shown in Table 1. For further discussion of our results, the study area has been defined as
280 a northern part (north of the mean position of Findlater Jet) including sites 21 °N, 19 °N, and
281 15 °N; and a southern part including sites 11 °N, and 13 °N (Fig. 1a).

282 3.1 Bulk sedimentary analysis and SST reconstruction

283 To compare with U_{37}^{kl} based-SST reconstruction, we present the SST values derived from
284 satellite data (Fig. 1b) averaged for the years 2017–2020. High spatial variability in SST is
285 observed from the north (mean 27.4°C) to the south (28°C). The surface chlorophylla (Chla)
286 value average from 2017-2020 is shown in Fig. 1c. A distinct north-south variability is noticed
287 with higher Chla values ($\sim 1\text{--}2 \text{ mg m}^{-3}$) in the north and lower values in the south ($\sim 0\text{--}0.5 \text{ mg}$
288 m^{-3}). TIC contents (Fig. 2a) are slightly higher in the south ($7.06 \pm 0.63 \%$) compared to the
289 north ($5.15 \pm 1.57 \%$) and this difference is statistically significant at a 94.7 % confidence level
290 (single factor ANOVA analysis, Table 2). TOC contents (Fig. 2b) are substantially higher (p
291 < 0.001) above 15° N ($0.97 \pm 0.06 \%$) reaching their highest value at 21° N and decreased
292 southward ($0.78 \pm 0.005 \%$). TN values (Fig. 2c) revealed a similar trend as TOC and decreased
293 from 21° N ($0.11 \pm 0.001 \%$) to 11° N ($0.07 \pm 0.009 \%$). The average TN value (0.06 ± 0.008
294 $\%$) in the south is significantly lower ($p < 0.001$) compared to the north ($0.087 \pm 0.018 \%$). The
295 ratio of TOC and TN (Table 1) is the lowest (9.5 ± 0.18) in the north at 21° N and increased at
296 the rest of the stations reaching > 12 . The U_{37}^{kl} based SST (Fig. 2d) shows an average value of
297 $27.8 \pm 0.3 \text{ }^\circ\text{C}$. The coolest reconstructed SSTs ($27.6 \pm 0.25 \text{ }^\circ\text{C}$) are found in the north and are
298 nearly $0.4 \text{ }^\circ\text{C}$ cooler compared to the south ($p < 0.05$) (Table 2).

299 3.2 Lipid biomarkers

300 The lipid biomarkers brassicasterol (Fig. 2e), dinosterol (Fig. 2f), dinostanol, the saturated,
301 degradative product of dinosterol (Fig. 2g), summed $\text{C}_{37:2}$ and $\text{C}_{37:3}$ alkenones (C_{37} alkenone) (Fig.
302 2h), cholesterol (Fig. 2i), and its degradative product cholestanol (Fig. 2j) are present in the
303 surface sediments from north to south.

304 Among phytoplankton lipid biomarkers, the average dinosterol contents ($98 \pm 64 \text{ ng g}^{-1}$) found
305 in the surface sediment are the highest followed by brassicasterol ($64 \pm 44 \text{ ng g}^{-1}$) and then C_{37}
306 alkenones ($39.4 \pm 12 \text{ ng g}^{-1}$) (Table 1) and show significant linear positive correlations (R^2
307 $= 0.62\text{--}0.96$, $p < 0.05$) with each other. All three biomarkers show the highest concentrations at
308 the northernmost station at 21° N (Fig. 2; Table 1) and decrease to their minimum values at 11°
309 N . The sum of the major biomarkers (brassicasterol, dinosterol, and alkenones) representing
310 the major three phytoplankton groups, with the highest concentrations ($33.9 \pm 14.13 \text{ } \mu\text{g g}^{-1}$
311 TOC) occur at 21° N compared to other stations ($19.96 \pm 9.5 \text{ } \mu\text{g g}^{-1}$ TOC) (Fig. 2). The TOC
312 normalized values of dinosterol ($16.53 \pm 8.3 \text{ } \mu\text{g g}^{-1}$ TOC) and brassicasterol ($12.37 \pm 5.2 \text{ } \mu\text{g g}^{-1}$
313 TOC) are the highest at the northernmost station and decrease southward. However, the
314 average values of dinosterol (north: $12.81 \pm 6.3 \text{ } \mu\text{g g}^{-1}$ TOC; south $7.8 \pm 4.47 \text{ } \mu\text{g g}^{-1}$ TOC) and
315 brassicasterol (north: $8.64 \pm 4.75 \text{ } \mu\text{g g}^{-1}$ TOC; south $5.81 \pm 3.48 \text{ } \mu\text{g g}^{-1}$ TOC) are not
316 significantly different ($p > 0.05$) (Table 2). The average ratios of dinosterol to brassicasterol and
317 brassicasterol to alkenones are 1.5 and 1.6 (Table 1), respectively, without any significant
318 north-south variability (Table 2). However, none of the biomarkers showed any statistically
319 significant difference in their TOC normalized values between the stations.

320 Cholesterol (Fig. 2i), mostly varied between $10 \pm 2.5 \text{ } \mu\text{g g}^{-1}$ TOC (north) and $14.3 \pm 5.8 \text{ } \mu\text{g g}^{-1}$
321 TOC (south) without any statistical significance. The TOC normalized values of cholestanol
322 (Fig. 2j) are lower in the northern ($11.8 \pm 6.3 \text{ } \mu\text{g g}^{-1}$ TOC) than in the southern part ($15.9 \pm$
323 $11.4 \text{ } \mu\text{g g}^{-1}$ TOC) and no significant correlation was noticed (Table 2).

324 3.3 Silicious organisms: Radiolarians and diatoms

325 Radiolarian abundance (Fig. 2k) in the central Arabian Sea varied between 1.07 and 2.13×10^4
326 individuals g^{-1} with the highest numbers at 13° N and the lowest at 21° N . Their occurrences
327 are found to be higher at the southern stations (1.84×10^4 individuals g^{-1}) compared to northern
328 stations (1.10×10^4 individuals g^{-1}) with statistical significance ($p < 0.05$) (Table 2). The

329 community is dominated by the genus *Tetrapyle* sp. and their abundance was higher in the
330 south.

331 Diatom frustules from the surface sediments show high spatial variability in both abundance
332 and diversity. The total frustule abundance in the central Arabian Sea (Supplementary Table 1;
333 Fig. 21) ranges between 2.78 and 6.36×10^4 valves g^{-1} . The highest frustule abundance is
334 observed at $19\text{--}21^\circ$ N and the least at 11° N. At station 19° N, the frustule abundance is the
335 highest ($6.36 \pm 0.2 \times 10^4$ valves g^{-1}) among all stations (Table 1). The frustule numbers found
336 in the north ($5.46 \pm 0.95 \times 10^4$ valves g^{-1}) are 1.67 times higher than in the south ($p < 0.01$).
337 Diatom frustule diversity has been calculated to understand the north-south distribution pattern
338 and the average Shannon–Wiener diversity index (H') is 1.6 ± 0.1 with the highest diversity at
339 21° N (1.8) (Supplementary Fig. 1). Microscopic analysis reveals a total of 23 genera, with 9
340 centric and 14 pennate diatoms. More than five-fold higher abundance of centric diatoms is
341 observed than pennate at all the locations ($p < 0.05$).

342 The overall diatom community in the sediment samples from the central Arabian Sea
343 (Supplementary Table 1; Fig. 3) is observed to be dominated by *Coscinodiscus* (40%),
344 *Thalassiosira* (34%), *Pseudo-nitzschia* (6%), *Rhizosolenia* (4%), *Hemidiscus* (4%),
345 *Thalassionema* (4%), and *Nitzschia* (3%). The northern stations are dominated by
346 *Coscinodiscus* sp., whereas the two southernmost stations are dominated by *Thalassiosira* sp.
347 In the north, the highest abundance (2.46×10^4 valves g^{-1}) of *Coscinodiscus* sp. was observed
348 ($p < 0.05$) with the least abundance at 11° N (0.61×10^4 valves g^{-1}). In the south, *Thalassiosira*
349 seemed to dominate (1.59×10^4 valves g^{-1}) without any statistical significance. The Bray-
350 Curtis similarity index usually indicates the similarity in the distribution pattern of different
351 diatom genera/species. The results reveal (Supplementary Fig. 2) that the two dominating
352 diatom genera, i.e. *Coscinodiscus* sp. and *Thalassiosira* sp. are grouped showing a similar
353 distribution pattern. The commonly occurring pennate diatom *Pseudo-nitzschia* is present
354 independently, whereas, *Rhizosolenia* and *Thalassionema* are grouped. The other two major
355 contributing diatom genera, *Hemidiscus* and *Nitzschia* reveal a similar pattern.

356 3.4 Statistical analyses

357 In the RDA biplot (Fig. 4), Axis 1 and 2 explained most of the variability ($\sim 97.2\%$). The biotic
358 variables and all other environmental parameters show a distinct association. Interestingly,
359 TOC, TN, the key phytoplankton biomarkers (dinosterol, brassicasterol, dinostanol, and
360 alkenones), along with diatom frustules abundance, and the major genera are grouped and are
361 at the opposite axis where TIC, SST, cholesterol, and radiolarian were together. The association
362 between the larger diatoms like *Coscinodiscus* and *Rhizosolenia* and organic matter including
363 brassicasterol depicts that the organic matter flux is coupled with diatom fluxes. The
364 positioning of *Thalassiosira* opposite these parameters also suggests that its abundance is
365 higher in the south associated with warmer SSTs. TOC: TN ratio and TIC along with SST are
366 found to be closely related in the RDA plot (Fig. 4).

367 4. Discussion

368 4.1 Physical forcing induced spatial variability in physicochemical properties

369 The alkenone-derived SST suggests a cooler northern part compared to the south along the
370 sampling transect (64° E, Fig. 2d). The annual average of satellite-derived SST also revealed a
371 similar trend. Such variability in SST from north to south could be attributed to monsoon wind
372 variability and related processes. During the summer monsoon, the physicochemical
373 parameters (wind speed, SST, nutrients, mixed layer depths [MLDs]) along 64° E show distinct
374 north-south demarcation due to the presence of the Findlater Jet (Findlater, 1971). In the
375 northern flank of this jet axis, the maximum influence of upwelling is evidenced by the

376 presence of cooler SSTs, high nutrient levels, and shallower MLDs (Silori et al., 2021;
377 Chowdhury et al., 2021; Chowdhury et al., 2024). Along the axis (~15–18° N) of the Jet the
378 highest wind speeds are recorded (Silori et al., 2021; Chowdhury et al., 2021; Chowdhury et
379 al., 2024). The coolest SST value at 15° N is most likely due to the advection of cool nutrient-
380 rich upwelled waters from the western coastal Arabian Sea (Bauer et al., 1991). Furthermore,
381 such high wind speeds for a prolonged period may also lead to evaporative heat loss leading to
382 a decrease in SST. Contrarily, in the south downwelling induced deeper MLDs (>100 m),
383 nutrient-poor waters along with higher SSTs are observed (Latasa and Bidigare, 1998;
384 Chowdhury et al., 2021; Silori et al., 2021). During the winter monsoon, surface circulation
385 reverses in this region, and in the northern Arabian Sea cold dry wind leads to evaporative
386 cooling and subsequent convection leading to cooler SSTs, and high nutrient levels. At the
387 same time, southern regions remain oligotrophic and warm. During the intermonsoon and
388 premonsoon, SST increases and nutrient level reduces substantially along the entire transect
389 (Prasannakumar and Narvekar, 2005). Consistent with this fact, the annual average satellite-
390 derived Chl a values (Fig. 1c) also indicated higher phytoplankton biomass in the north induced
391 by nutrient enrichment, whereas the south was mostly low productive.

392 **4.2 Spatial variability in particle flux, and phytoplankton dynamics**

393 **4.2.1 Organic matter**

394
395 The northernmost stations were the hotspots for particulate organic matter (POM) flux and sink
396 to the sediment floor (Fig. 2). The positioning of SST in the RDA plot (Fig. 4) opposite TOC,
397 TN, diatom frustules, and phytoplankton lipid biomarkers also supported this fact. The north-
398 south variability in phytodetritus flux could be also influenced by dissolved oxygen levels
399 within the mesopelagic zone (Fig. 5) as it directly controls microbial degradation and
400 zooplankton activity (Moriceau et al., 2018; Iversen, 2023). In our sampling transect, the
401 northern stations are under the influence of intense oxygen deficiency which decreases in
402 intensity and thickness towards the south (Banse et al., 2014). In their synthesis, Banse et al.
403 (2014) showed that the median DO values within 150–500 m depth in the northern stations
404 within the core OMZ vary between 0.04 and 0.30 mL L⁻¹. Conversely, in the south, these values
405 increased to 0.24–0.72 mL L⁻¹. Such spatial variability in OMZ distribution/intensity across
406 the stations could substantially alter the rate of organic matter mineralization, zooplankton
407 abundance (Cavan et al., 2017), and particle flux attenuation (François et al., 2002; Keil et al.,
408 2016). Fast and efficient mineralization within the mesopelagic may allow less organic matter
409 to be transported, whereas partial remineralization may lead to higher organic matter export
410 flux (Ragueneau et al., 2006). Therefore, the northern stations at an intense OMZ may have a
411 higher preservation potential of organic matter compared to the south (Fig. 5) as mentioned by
412 Schulte et al. (2000).

413

414 **4.2.2 Lipid biomarkers as indicators of phytoplankton and zooplankton**

415 Phytoplankton and zooplankton produce specific lipid biomarkers that are stored in ocean
416 sediments (Castañeda and Schouten, 2011; Meyer 1997; Volkman et al., 1998; Volkman, 2003)
417 and are commonly used to reconstruct past environmental changes (Castañeda and Schouten,
418 2011; Eglinton and Eglinton, 2008). For instance, calcifying nanophytoplankton *Gephyrocapsa*
419 *huxleyi* (also known as *Emiliana huxleyi*) and *Gephyrocapsa oceanica* are known to be the
420 main producers of C₃₇ (C_{37:2} and C_{37:3}) alkenones in the ocean (Brassell et al., 1986; Eglinton
421 and Eglinton, 2008; Prahl and Wakeham, 1987). In modern and past climate studies C_{37:2} and
422 C_{37:3} alkenones are used extensively as reliable SST proxies (Prahl et al., 1988; Sonzogni et al.,
423 1997). Among sterols, dinosterol and its degradative product dinostanol are often used as a
424 proxy to represent dinoflagellates (Meyers, 1997; Castañeda and Schouten, 2011).

425
426 Brassicasterol a commonly used biomarker of diatoms, may be produced by other microalgae
427 (Volkman et al., 1998). For example, haptophytes and dinoflagellates produce minor contents
428 of brassicasterol, depending on physicochemical parameters like nutrient availability and
429 temperature (Ding et al., 2019). Brassicasterol contents could be higher in diatoms under a
430 balanced N:P supply, whereas a reduced N:P leads to higher brassicasterol production in
431 dinoflagellates (Ding et al., 2019). Nevertheless, brassicasterol is produced by most of the
432 pennate diatoms as major sterol, however, the quantity may vary substantially in radial centric
433 diatoms (Véron et al., 1998). Although we do not have enough experimental/field evidence to
434 disapprove that brassicasterol is produced solely by diatoms and hence could be a valid proxy
435 for this group, several studies show that many diatoms produce brassicasterol in significant
436 amounts, specifically pennates and also many radial centric diatoms (Véron et al. 1998; Ding
437 et al., 2019; Jaramillo-Madrid, et al., 2019; Jaramillo-Madrid, et al., 2020). Likewise, we are
438 using brassicasterol to indicate the presence of diatoms as a group in the sedimentary organic
439 matter without assigning this lipid biomarker to any specific phylogenetic group, genera, or
440 species to indicate the sources.

441 TOC-normalized lipid biomarker contents indicate the relative contribution of major
442 phytoplankton groups to total organic matter found in surface sediments. Both total and TOC-
443 normalized phytoplankton lipid biomarkers revealed that dinoflagellates, diatoms, and
444 coccolithophores were the dominant phytoplankton groups (Fig. 2). All studies available from
445 the Arabian Sea using biomarkers (Schubert et al., 1998; Schulte et al., 1999; 2000; Prahl et
446 al., 2000) showed that dinosterol contents were higher than brassicasterol, both in sediment
447 core and trap samples, suggesting greater contributions of dinoflagellates compared to diatoms.
448 Likewise, we also observed nearly 1.5 times higher dinosterol contents compared to
449 brassicasterol. The dominance of dinosterol, C₃₇-alkenones, and some species-specific lipid
450 biomarkers for diatoms was found in sediment trap samples (2220 m depth) from the central
451 (Prahl et al., 2000), in two sediment core samples from the northeastern and southern Arabian
452 Sea (Schulte et al., 1999). Further, a long sediment core from the northern Arabian Sea close
453 to our sampling locations (22° 29.31' N, 65° 38.9' E) (Schubert et al., 1998) also reported the
454 same dominating phytoplankton groups in the Arabian Sea over the past 0.2 million years.

455
456 Since diatoms predominate over dinoflagellates during phytoplankton blooms (Chowdhury et
457 al., 2021; 2024) a higher contribution of brassicasterol over dinosterol should be expected,
458 however, it was the opposite in our study. This reverse trend can be explained by the seasonal
459 succession of phytoplankton communities in surface layers mostly driven by nutrient
460 stoichiometry related to monsoon wind forcings and grazing (Prahl et al., 2000; Rixen et al.,
461 2019a). It should be noted that organic matter on the surface sediment accumulates throughout
462 the year with variable depositional rates. Monsoon reversal also leads to changes in the
463 phytoplankton community (Sawant and Madhupratap, 1996; Latasa and Bidigare, 1998) that
464 may also affect the transfer of phytodetritus to the sea floor. Consequently, diatom frustules
465 largely represent the signature of the most productive seasons. In contrast, the nutrient-poor
466 phases are usually dominated by dinoflagellates and other calcifying nanophytoplankton.
467 Dinoflagellates grow slowly in nutrient-poor warm waters and can remain there for longer
468 periods (k-strategists) (Smayda and Reynolds, 2001; Glibert et al., 2016). Likewise, this
469 situation can be found at the southern stations, where high SSTs and oligotrophic conditions
470 were more favorable for the growth of dinoflagellates (Chowdhury et al., 2021; 2024). This is
471 reflected south of the 15° N station by the occurrences of dinoflagellates like *Gymnodinium*
472 sp., *Gyrodinium* sp, and *Katodinium* sp. with small cells (Garrison et al., 1998; Chowdhury et
473 al., 2021).

474 Moreover, unlike diatoms, which are photoautotrophs, most dinoflagellates could be either
475 heterotrophs or mixotrophs (Stoecker, 1999; Stoecker et al., 2017) which actively graze on
476 smaller phytoplankton including diatoms and even could be detritivorous feeding on particles
477 (García-Oliva et al., 2022). Mixotrophs could consume prey to meet their cellular nitrogen
478 demand and can simultaneously perform photosynthesis to gain carbon (Stoecker et al., 2017).
479 In the Arabian Sea, a significant part of the dissolved inorganic nitrogen is lost due to strong
480 denitrification within the OMZ and often becomes the growth-limiting nutrient for
481 phytoplankton (Ward et al., 2006). Therefore, particularly during the stratified oligotrophic
482 phases like intermonsoon and premonsoon, when SST increases fostering stratification,
483 nanophytoplankton, and dinoflagellates dominate over diatoms. Hence, the overall contribution
484 of dinoflagellates on an annual basis could exceed diatoms as dinoflagellates are constantly
485 present during both high-nutrient regimes and low-nutrient stratified warm water periods.

486 Another possible factor for the observed variability in brassicasterol to dinosterol could be due
487 to differences in their labile nature. It was claimed that diatom-rich organic matter could be of
488 higher lability (François et al., 2002) and may possess low transfer potential to the sea floor
489 (Alonso-González et al., 2010). Contrary to this, it was also observed that compared to other
490 phytoplankton (Cabrera-Brufau et al., 2021) diatom-rich organic matter is more of a refractory
491 nature against mesopelagic microbial degradation. Moreover, the phytodetritus of diatom
492 origin could be preferably consumed by the benthic communities than other phytoplankton
493 groups (Nomaki et al., 2021) and could be one of the reasons for lower brassicasterol over
494 dinosterol in the surface sediment. This is indeed difficult to conclude as we do not have enough
495 experimental evidence supporting/contradicting these hypotheses. Further, as mentioned
496 before we can not exclude, that brassicasterol is sourced by other phytoplankton groups than
497 diatoms.

498 In the central Arabian Sea, coccolithophores constitute an important part of the
499 nanophytoplankton community (Andruleit et al., 2004; Schiebel et al., 2004; Mergulhao et al.,
500 2006). The relatively high occurrences of substantial amounts of C₃₇-alkenones all along the
501 transect in our study indicate that coccolithophores may also contribute as a major part of
502 sinking phytodetritus, with slightly higher values towards the north (Fig. 2h). Sediment trap
503 studies from the south of the Findlater Jet (Mergulhao et al., 2006) reported the flux of
504 coccolithophores throughout the year justifying our observations.

505 **4.2.3 Diatom frustules**

506 In our previous study (Pandey et al., 2023), using the topmost (0–0.5 cm) part of the cores, a
507 trend in diatom frustule abundance and diversity from north to south was observed. After
508 compiling the data from 0.5 to 1 cm a similar trend was noticed. The highest abundance of
509 diatom frustules coupled with TOC and TN contents was found in the northern stations, which
510 most likely indicated higher organic matter transfer to the sediment compared to the southern
511 stations. The RDA plot (Fig. 4) also revealed that the abundance of large centric diatoms like
512 *Coscinodiscus*, *Rhizosolenia*, TOC, and TN contents as well as brassicasterol were grouped
513 and correlated significantly. In this context, it should be noted that the correlation between
514 brassicasterol and the major diatom taxa does not necessarily suggest that they are the sole
515 producers of this lipid biomarker as mentioned in the previous sections. This correlation most
516 probably indicates that the highest production of brassicasterol and diatom bloom might have
517 cooccurred and during this period, large diatoms like *Rhizosolenia* or *Coscinodiscus* also
518 dominated with many other centric and pennate diatoms that produce brassicasterol.

519 During both summer (Chowdhury et al., 2021) and winter monsoons (Sawant and
520 Madhupratap, 1996) in the northern Arabian Sea, *Coscinodiscus* and *Rhizosolenia* are the

521 major diatoms forming blooms and consequently, dominate the flux of biogenic silica (Rixen
522 et al., 2019a). A higher abundance of large *Rhizosolenia* frustules was also seen in the sediment
523 trap samples from the central Arabian Sea after the summer monsoon bloom (Rixen et al.,
524 2019a). The contribution of heavily silicified diatom frustules may in addition provide
525 ballasting effects (Smetacek, 1985; Tréguer et al., 2018) facilitating efficient organic matter
526 export compared to other phytoplankton groups (Buesseler, 1998; Boyd and Newton, 1999;
527 Zúñiga et al., 2021). Diatom bloom development in the Arabian Sea was found to be associated
528 with dissolved silica (DSi) availability (Chowdhury et al., 2021) and the depth of the silicicline
529 (Anju et al., 2020). The northern stations become DSi depleted ($<2 \mu\text{M}$) at the end of the bloom
530 (Chowdhury et al., 2021) and may lead to a mass sinking of frustules (Smetacek, 1985; Krause
531 et al., 2019) or they can be grazed and cell death may also occur due to viral attacks (Agusti
532 and Duarte, 2000). On the other hand, the abundance of small chain-forming diatoms such as
533 *Thalassiosira*, *Pseudo-nitzschia*, *Nitzschia*, and *Thalassionema*, enhanced in the surface
534 sediment in the southern stations (Fig. 3). Low nutrient conditions prevail in this region even
535 during summer and winter monsoons. During the intermonsoon and premonsoon oligotrophy
536 intensifies in these regions supporting the growth of smaller diatoms or non-diatoms (Garrison
537 et al., 1998; Tarran et al., 1999; Chowdhury et al., 2021) that could sink slower compared to
538 the larger cells in the north (Buesseler and Boyd, 2009).

539 Moreover, diatom frustules may dissolve while sinking and some of them (e. g. thickly
540 silicified frustules) reach the abyssal plain and are preserved in the seafloor sediments.
541 Nevertheless, the organic coating that protects siliceous frustules from dissolution (Lewin,
542 1961), can be degraded by heterotrophic bacterial activity (Bidle and Azam, 1999; Roubex et
543 al., 2008). The presence of OMZ in the northern stations (200–1200 m) could therefore slow
544 down such dissolution facilitating frustules to reach the sea floor. On the other hand, in the
545 south, small and thinly silicified diatom frustules (mostly due to DSi limitation) may be more
546 fragile as they travel through the well-oxygenated water column and higher heterotrophic
547 activity may enhance the risk of degradation leading to reduced frustules abundance on the
548 seabed. In addition to this, the almost 700 m deeper water column in the south compared to the
549 north could enhance the scope of degradation of sinking particles. This is consistent with our
550 observation.

551 **4.2.4 Zooplankton grazing**

552
553 Two proxies representing zooplankton have been considered in this study 1) sterol biomarkers
554 [cholesterol (Fig. 2i), and its degradative product cholestanol (Fig. 2j)], and 2) radiolarians
555 (Fig. 2k). Cholesterol and cholestanol are produced in high amounts by zooplankton and are
556 used as zooplankton proxies, nevertheless, some phytoplankton may also produce them in
557 insignificant quantities (Kohlbach et al., 2021; Taipale et al., 2016; Wittenborn et al., 2020).
558 Accordingly, the highest concentration of TOC-normalized cholesterol was found in the south
559 indicating more zooplankton activity. In the RDA biplot, SST was grouped with cholestanol
560 and was on the same side as cholesterol indicating higher zooplankton activity in the south.
561 The association of TIC with cholesterol indicates that calcareous zooplankton could also be a
562 source of cholesterol. Consequently, a higher fecal matter production could enhance particle
563 flux compared to the north. Nonetheless, a major part of the fecal matter could also be degraded
564 within the upper mesopelagic layer as reported by Iversen et al. (2017). In the Southern Ocean,
565 more than 87% of fecal matter produced in the surface ocean can be lost via remineralization
566 before reaching the upper mesopelagic zone (300 m) (Iversen et al. 2017). Likewise, the
567 warmer temperature in the mesopelagic water column at our sampling locations could facilitate
568 faster mineralization. Zooplankton grazing could largely alter the magnitude of carbon export
569 flux (Moriceau et al., 2018). Thus, the low abundance of mesozooplankton within the OMZ
570 may decrease defragmentation, which in turn slows down the bacterial remineralization of

571 phytodetritus allowing a higher amount of carbon to be exported to the abyssal plain (Cavan et
572 al., 2017) (Fig. 5). Likewise, the lower zooplankton activity in the mesopelagic OMZ of the
573 Arabian Sea (Wishner et al., 1998) may hinder particle fragmentation that usually accelerates
574 degradation (Briggs et al., 2020). Similarly, at the northern stations, lower zooplankton
575 abundance within the OMZ (Cavan et al., 2017) may restrict particle flux attenuation (Fig. 5).

576 In the western and central Arabian Sea, 50–100% of the diatom population can be grazed by
577 copepods (Landry et al., 1998; Smith et al., 1998; Gauns et al., 2005). Importantly, diatom cell
578 size can be a crucial factor that determines their grazing rates. Copepods exhibit the highest
579 grazing rate when the ratio between prey and predator body size remains 18:1 on average
580 (Hansen et al., 1994). In the north and at the axis of the Findlater Jet, the higher availability of
581 nutrients, particularly DSi could promote large and thickly silicified diatoms which are difficult
582 to graze for copepods (Hansen et al., 1994; Ryderheim et al., 2022). Subsequently, large centric
583 diatoms like *Coscinodiscus radiatus* and *Rhizosolenia* spp. could escape grazing by copepods
584 (Jansen, 2008; Löder et al., 2011) and can sink to the seafloor (Buesseler and Boyd, 2009;
585 Kemp et al., 2006). On the contrary, the bloom-forming diatoms with thinly silicified frustules
586 like *Chaetoceros* and *Leptocylindrus* (Sawant and Madhupratap, 1996; Chowdhury et al.,
587 2021) can be grazed easily and are usually not found in the sediment. However, the lipid
588 biomarkers of these diatoms (brassicasterol) may be preserved after transport through the water
589 column in fecal pellets in surface sediments. In the case of the southern stations, smaller
590 diatoms or non-diatoms could be consumed by microzooplankton (Swanberg and Anderson,
591 1985). Corroborating with this fact, the significantly higher number of radiolarians (Fig. 2k)
592 which mostly consume smaller phytoplankton, bacterioplankton, and copepods (Caron et al.,
593 1995) were higher in the south. A high abundance of radiolarians dominated by *Tetrapyle* sp.
594 that are found under high salinity was also reported by a previous study from the Arabian Sea
595 (Gupta, 2003).

596

597 **4.3 Influence of lateral advection**

598

599 Since there is evidence of advected waters reaching from the western Arabian Sea to its central
600 part, the chances of particle transport also need to be considered. Stable nitrogen isotopic values
601 of particulate organic matter ($\delta^{15}\text{N}_{\text{POM}}$, Silori et al., 2021) revealed that nutrient enrichment
602 mostly takes place via advection from the upwelling system as well as entrainment close to the
603 axis of the Findlater Jet (16–18° N). Earlier studies also noticed the presence of slightly low
604 saline waters in this region probably due to advection from the western Arabian Sea (Prasanna
605 Kumar et al., 2000). Additionally, Silori et al. (2021) reported lower $\delta^{15}\text{N}$ values of particulate
606 nitrogen during summer monsoon at the stations influenced by the axis suggesting laterally
607 advected dissolved inorganic nitrogen from the Somali upwelling region. However, so far there
608 is no report claiming that particulate organic matter can be advected such a long distance (~600
609 km) without being grazed/remineralized/sinking. Contrarily, there is plenty of evidence
610 showing a direct relation between phytoplankton bloom and particle flux in these regions
611 (Haake et al., 1993; Rixen et al., 2019a). Thus, the possibility of lateral transport of
612 phytoplankton or detritus from the western Arabian Sea to the seabed of the central Arabian
613 Sea may be overlain by vertical particle flux.

614

615 **Conclusions**

616 In our previous study (Pandey et al., 2023) using diatom frustules and sedimentary bulk
617 parameters from the topmost part of the sediment core (0–0.5 cm), we established a link
618 between the spatial trend in organic matter variability, atmospheric forcing, and phytoplankton

619 bloom. The present study aims for the first time to elucidate phytoplankton-driven particle flux
620 to the seafloor using sedimentary lipid biomarkers from the central Arabian Sea. Such studies
621 linking sedimentary organic matter to physical forcings and phytoplankton community have
622 rarely been conducted in the central Arabian Sea. Importantly, most of the studies using
623 sediment traps focused on diatoms and coccolithophores, but neglected dinoflagellates (Nair et
624 al., 1989). A few studies proposed that the diatom blooms could be replaced by dinoflagellates.
625 On the other hand, another study (Schubert et al., 1998), revealed that the relative contribution
626 of dinosterol was higher than brassicasterol over the last 0.2 million years in this basin.
627 Following this concept, we crosschecked the organic matter from the top 1 cm of surface
628 sediments from more locations across a spatially variable transect (from high to low
629 productive).

630 Our results indicated that dinoflagellates have contributed more to the sedimentary
631 phytodetritus compared to diatoms even in the recent past. We propose that diatoms and
632 coccolithophores do contribute to sedimentary particle flux. However, the dinoflagellates
633 dominate due to their survival strategies during poor nutrient supply. We show that the distinct
634 spatial variability in physical forcing drives the phytoplankton bloom and the particle flux is
635 also closely coupled. Nevertheless, we also need to mention that the diatom community
636 constructed from the frustules is not the direct producer of brassicasterol; the community
637 provides more information about the surface oceanic processes including nutrient availability.
638 The northernmost station in the central Arabian Sea was found to be a hotspot for sinking
639 particles followed by subsequent preservation mostly due to the prevailing OMZ (Fig. 5). Both
640 summer and winter monsoon-induced phytoplankton bloom dominated by diatoms led to the
641 sinking of large thickly silicified frustules on the sediment floor. We hypothesized that the low
642 oxygen within the thick OMZ could slow down the dissolution of frustules as well as
643 heterotrophic degradation and fragmentation by zooplankton leading to low flux attenuation.
644 Contrarily, in the south, higher dissolved oxygen levels could facilitate faster remineralization
645 and higher zooplankton activity resulting in more flux attenuation and reduced particle
646 transport to the sea floor. Contrary to the global scenario of expanding OMZs, a few recent
647 studies (Vallivattathillam et al., 2023; Liu et al., 2024) showed that the southern part of the
648 OMZ can get thinner in the future due to the higher supply of oxygen. Such changes could
649 facilitate higher heterotrophic activities within the mesopelagic and thus could impact particle
650 flux attenuation in this region and need to be investigated.

651 **Acknowledgments**

652 MP was supported by the Department of Science and Technology (DST) - Inspire Fellowship.
653 This study is an outcome of the CSIR-NIO in-house program “Impact of Climate Change on
654 the Physics, Biogeochemistry, and the Ecology of the North Indian Ocean (ClicNIO)” (MLP
655 1802) funded by the Council of Scientific and Industrial Research (CSIR). We express our
656 gratitude to the captain, scientists, technical staff, ship cell staff, deckhands, and the students
657 onboard *RV Sindhu Sadhana* (SSD 068) for their constant help and support during the cruise.
658 We are thankful to the Director, CSIR NIO for his kind support. Ms. Teja Naik is acknowledged
659 for her technical help in using the Coulometer under the central analytical facility in CSIR,
660 NIO, Goa. The contribution number is XXXX. NB was funded by the Deutsche
661 Forschungsgemeinschaft (DFG, German Research Foundation) under Germany’s Excellence
662 Strategy – EXC 2037 'CLICCS - Climate, Climatic Change, and Society' – Project Number:
663 390683824, contribution to the Center for Earth System Research and Sustainability (CEN) of
664 Universität Hamburg.

665

666 **Availability of data and materials:** The data are available online at Mendeley Data (DOI:
667 10.17632/xm4nxzdx2.1)

668 **Statements and Declarations**

669 **Competing Interests:** *The authors have no relevant financial or non-financial interests to*
670 *disclose.*

671 **Ethical Approval: Not applicable**

672 **Consent to Participate: Not applicable**

673 **Consent to Publish: Not applicable**

674 **Authors' Contributions:** *MP: Conceptualization, sampling, sample analysis; formal*
675 *analysis, data curation, writing original manuscript and editing; HB: Conceptualization; Fund*
676 *acquisition; sampling; manuscript reviewing and editing; DB: sampling; manuscript*
677 *reviewing and editing NB: Sample analysis, Conceptualization; manuscript reviewing and*
678 *editing BG: Conceptualization; reviewing and editing*

679 **References**

- 680 1. Abrantes, F.F.G. and Sancetta, C.: Diatom assemblages in surface sediments reflect
681 coastal upwelling off southern Portugal, *Oceanologica acta*, 8,7–12, 1985.
- 682 2. Agustí, S. and Duarte, C.M.: Strong seasonality in phytoplankton cell lysis in the NW
683 Mediterranean littoral, *Limnology and Oceanography*, 45, 940–947,
684 <https://doi.org/10.4319/lo.2000.45.4.0940>, 2000.
- 685 3. Alonso-González, I.J., Arístegui, J., Lee, C., Sanchez-Vidal, A., Calafat, A., Fabrés, J.,
686 Sangrá, P., Masqué, P., Hernández-Guerra, A. and Benítez-Barrios, V.: Role of slowly
687 settling particles in the ocean carbon cycle, *Geophysical research letters*, 37,
688 <https://doi.org/10.1029/2010GL043827>, 2010.
- 689 4. Andruleit, H., Rogalla, U. and Stäger, S.: From living communities to fossil
690 assemblages: origin and fate of coccolithophores in the northern Arabian Sea,
691 *Micropaleontology*, 50, 5-21, https://doi.org/10.2113/50.Suppl_1.5, 2004.
- 692 5. Anju, M., Sreeush, M.G., Valsala, V., Smitha, B.R., Hamza, F., Bharathi, G. and Naidu,
693 C.V.: Understanding the role of nutrient limitation on plankton biomass over Arabian
694 Sea via 1-D coupled biogeochemical model and bio-Argo observations, *Journal of*
695 *Geophysical Research: Oceans*, 125, e2019JC015502,
696 <https://doi.org/10.1029/2019JC015502>, 2020.
- 697 6. Armbrrecht, L.H., Lowe, V., Escutia, C., Iwai, M., McKay, R. and Armand, L.K.:
698 Variability in diatom and silicoflagellate assemblages during mid-Pliocene glacial-
699 interglacial cycles determined in Hole U1361A of IODP Expedition 318, Antarctic
700 Wilkes Land Margin, *Marine Micropaleontology*, 139, 28–41,
701 <https://doi.org/10.1016/j.marmicro.2017.10.008>, 2018.
- 702 7. Banse, K.: Seasonality of phytoplankton chlorophyll in the central and northern
703 Arabian Sea, *Deep Sea Research Part A, Oceanographic Research Papers*, 34, 713–723,
704 [https://doi.org/10.1016/0198-0149\(87\)90032-X](https://doi.org/10.1016/0198-0149(87)90032-X), 1987.
- 705 8. Banse, K., Naqvi, S.W.A., Narvekar, P.V., Postel, J.R. and Jayakumar, D.A.: Oxygen
706 minimum zone of the open Arabian Sea: variability of oxygen and nitrite from daily to
707 decadal timescales, *Biogeosciences*, 11, 2237–2261, [https://doi.org/10.5194/bg-11-](https://doi.org/10.5194/bg-11-2237-2014)
708 [2237-2014](https://doi.org/10.5194/bg-11-2237-2014), 2014.
- 709 9. Barnett, P.R.O., Watson, J. and Connelly, D.: A multiple corer for taking virtually
710 undisturbed samples from shelf, bathyal and abyssal sediments, *Oceanologica acta*, 7,
711 399–408, 1984.
- 712 10. Bauer, S., Hitchcock, G.L., Olson, D.B.: Influence of monsoonally-forced Ekman
713 dynamics upon surface layer depth and plankton biomass distribution in the Arabian

- 714 Sea, Deep Sea Research, Part A Oceanographic Research Papers 38, 531–553,
715 [https://doi.org/10.1016/0198-0149\(91\)90062-K](https://doi.org/10.1016/0198-0149(91)90062-K), 1991.
- 716 11. Behrenfeld, M.J., O'Malley, R.T., Siegel, D.A., McClain, C.R., Sarmiento, J.L.,
717 Feldman, G.C., Milligan, A.J., Falkowski, P.G., Letelier, R.M. and Boss, E.S.: Climate-
718 driven trends in contemporary ocean productivity, *Nature*, 444, 752–755,
719 <https://doi.org/10.1038/nature05317>, 2006.
- 720 12. Bhattathiri, P.M.A., Pant, A., Sawant, S., Gauns, M., Matondkar, S.G.P. and
721 Mohanraju, R.: Phytoplankton production and chlorophyll, *Current Science*, 71, 1996.
- 722 13. Bidle, K.D. and Azam, F.: Accelerated dissolution of diatom silica by marine bacterial
723 assemblages, *Nature*, 397, 508–512, <https://doi.org/10.1038/17351>, 1999.
- 724 14. Boyd, P.W. and Newton, P.P.: Does planktonic community structure determine
725 downward particulate organic carbon flux in different oceanic provinces?, *Deep Sea*
726 *Research Part I: Oceanographic Research Papers*, 46, 63–91,
727 [https://doi.org/10.1016/S09670637\(98\)00066-1](https://doi.org/10.1016/S09670637(98)00066-1), 1999.
- 728 15. Brassell, S.C., Brereton, R.G., Eglinton, G., Grimalt, J., Liebezeit, G., Marlowe, I.T.,
729 Pflaumann, U. and Sarnthein, M.: Palaeoclimatic signals recognized by chemometric
730 treatment of molecular stratigraphic data, *Organic Geochemistry*, 10(4-6), 649–660,
731 [https://doi.org/10.1016/S0146-6380\(86\)80001-8](https://doi.org/10.1016/S0146-6380(86)80001-8), 1986.
- 732 16. Briggs, N., Dall'Olmo, G. and Claustre, H.: Major role of particle fragmentation in
733 regulating biological sequestration of CO₂ by the oceans, *Science*, 367, 791–793,
734 <https://doi.org/10.1126/science.aay1790>, 2020.
- 735 17. Buesseler, K.O. and Boyd, P.W.: Shedding light on processes that control particle
736 export and flux attenuation in the twilight zone of the open ocean, *Limnology and*
737 *Oceanography*, 54, 1210–1232, <https://doi.org/10.4319/lo.2009.54.4.1210>, 2009.
- 738 18. Buesseler, K.O.: The decoupling of production and particulate export in the surface
739 ocean, *Global Biogeochemical Cycles*, 12, 297–310,
740 <https://doi.org/10.1029/97GB03366>, 1998.
- 741 19. Cabrera-Brufau, M., Arin, L., Sala, M.M., Cermeño, P. and Marrasé, C.: Diatom
742 dominance enhances resistance of phytoplanktonic POM to mesopelagic microbial
743 decomposition, *Frontiers in Marine Science*, 8, p.683354,
744 <https://doi.org/10.3389/fmars.2021.683354>, 2021.
- 745 20. Caron, D.A., Michaels, A.F., Swanberg, N.R. and Howse, F.A.: Primary productivity
746 by symbiont-bearing planktonic sarcodines (Acantharia, Radiolaria, Foraminifera) in
747 surface waters near Bermuda, *Journal of Plankton Research*, 17, 103–129.
748 <https://doi.org/10.1093/plankt/17.1.103>, 1995.
- 749 21. Castañeda, I.S. and Schouten, S.: A review of molecular organic proxies for examining
750 modern and ancient lacustrine environments, *Quaternary Science Reviews*, 30(21-22),
751 2851–289, <https://doi.org/10.1016/j.quascirev.2011.07.009>, 2011.
- 752 22. Cavan, E.L., Trimmer, M., Shelley, F. and Sanders, R.: Remineralization of particulate
753 organic carbon in an ocean oxygen minimum zone. *Nature Communications*, 8(1),
754 p.14847, <https://doi.org/10.1038/ncomms14847>, 2017.
- 755 23. Chowdhury, M., Biswas, H., Mitra, A., Silori, S., Sharma, D., Bandyopadhyay, D.,
756 Shaik, A.U.R., Fernandes, V. and Narvekar, J.: Southwest monsoon-driven changes in
757 the phytoplankton community structure in the central Arabian Sea (2017–2018): After
758 two decades of JGOFS, *Progress in Oceanography*, 197, p.102654,
759 <https://doi.org/10.1016/j.pocean.2021.102654>, 2021.
- 760 24. Chowdhury, M., Biswas, H., Silori, S. and Sharma, D.: Spatiotemporal variability in
761 phytoplankton size class modulated by summer monsoon wind forcing in the central
762 Arabian Sea, *Journal of Geophysical Research: Oceans*, 129, e2023JC019880,
763 <https://doi.org/10.1029/2023JC019880>, 2024.

- 764 25. Copernicus Climate Change Service (C3S), ERA5: Fifth generation of ECMWF
765 atmospheric reanalyses of the global climate, Copernicus Climate Change Service
766 Climate Data Store (CDS), 2017.
- 767 26. Desikachary, T.V.: Atlas of Diatoms (Marine Diatoms of the Indian Ocean Region), 6,
768 Madras Science Foundation, Madras Fasc, 1–13, 1989.
- 769 27. Ding, Y., Bi, R., Sachs, J., Chen, X., Zhang, H., Li, L. and Zhao, M., Lipid biomarker
770 production by marine phytoplankton under different nutrient and temperature regimes.
771 Organic Geochemistry, 131, 34-49. <https://doi.org/10.1016/j.orggeochem.2019.01.008>,
772 2019.
- 773 28. Eglinton, T.I. and Eglinton, G., 2008. Molecular proxies for paleoclimatology, Earth
774 and Planetary Science Letters, 275(1–2), 1–16,
775 <https://doi.org/10.1016/j.epsl.2008.07.012>, 2008.
- 776 29. Engel, A., Wagner, H., Le Moigne, F.A. and Wilson, S.T.: Particle export fluxes to the
777 oxygen minimum zone of the eastern tropical North Atlantic, Biogeosciences, 14,1825-
778 1838, <https://doi.org/10.5194/bg-14-1825-2017>, 2017.
- 779 30. Field, C.B., Behrenfeld, M.J., Randerson, J.T. and Falkowski, P.: Primary production
780 of the biosphere: integrating terrestrial and oceanic components, Science, 281, 237–
781 240, <https://doi.org/10.1126/science.281.5374.237>, 1998.
- 782 31. Findlater, J.: Mean monthly airflow at low levels over the western Indian Ocean (No.
783 116). HM Stationery Office, Pure Appl. Geophys. PAGEOPH 115, 1251–1262,
784 <https://doi.org/10.1007/BF00874408>, 1971.
- 785 32. Francois, R., Honjo, S., Krishfield, R. and Manganini, S.: Factors controlling the flux
786 of organic carbon to the bathypelagic zone of the ocean, Global Biogeochemical
787 Cycles, 16, 34–1, <https://doi.org/10.1029/2001GB001722>, 2002.
- 788 33. García-Oliva, O., Hantzschke, F.M., Boersma, M. and Wirtz, K.W.: Phytoplankton and
789 particle size spectra indicate intense mixotrophic dinoflagellates grazing from summer
790 to winter. Journal of Plankton Research, 44, 224–240,
791 <https://doi.org/10.1093/plankt/fbac013>, 2022.
- 792 34. Garrison, D.L., Gowing, M.M. and Hughes, M.P.: Nano-and microplankton in the
793 northern Arabian Sea during the Southwest Monsoon, August–September 1995 A US–
794 JGOFS study, Deep Sea Research Part II: Topical Studies in Oceanography, 45, 2269–
795 2299, [https://doi.org/10.1016/S0967-0645\(98\)00071-X](https://doi.org/10.1016/S0967-0645(98)00071-X), 1998.
- 796 35. Gauns, M., Madhupratap, M., Ramaiah, N., Jyothibabu, R., Fernandes, V., Paul, J.T.
797 and Kumar, S.P.: Comparative accounts of biological productivity characteristics and
798 estimates of carbon fluxes in the Arabian Sea and the Bay of Bengal. Deep Sea Research
799 Part II: Topical Studies in Oceanography, 52, 2003–2017,
800 <https://doi.org/10.1016/j.dsr2.2005.05.009>, 2005.
- 801 36. Glibert, P.M., Wilkerson, F.P., Dugdale, R.C., Raven, J.A., Dupont, C.L., Leavitt, P.R.,
802 Parker, A.E., Burkholder, J.M. and Kana, T.M.: Pluses and minuses of ammonium and
803 nitrate uptake and assimilation by phytoplankton and implications for productivity and
804 community composition, with emphasis on nitrogen-enriched conditions, Limnology
805 and Oceanography, 61, 165–197, <https://doi.org/10.1002/lno.10203>, 2016.
- 806 37. Gupta, S.M.: Orbital frequencies in radiolarian assemblages of the central Indian
807 Ocean: implications on the Indian summer monsoon, Palaeogeography,
808 Palaeoclimatology, Palaeoecology, 197(1-2), 97–112, [https://doi.org/10.1016/S0031-0182\(03\)00388-2](https://doi.org/10.1016/S0031-0182(03)00388-2), 2003.
- 810 38. Haake, B., Ittekkot, V., Rixen, T., Ramaswamy, V., Nair, R.R. and Curry, W.B.:
811 Seasonality and interannual variability of particle fluxes to the deep Arabian Sea, Deep
812 Sea Research Part I: Oceanographic Research Papers, 40(7), 1323–1344,
813 [https://doi.org/10.1016/0967-0637\(93\)90114-I](https://doi.org/10.1016/0967-0637(93)90114-I), 1993.

- 814 39. Hansen, B., Bjornsen, P.K. and Hansen, P.J.: The size ratio between planktonic
815 predators and their prey, *Limnology and oceanography*, 39(2), 395–403,
816 <https://doi.org/10.4319/lo.1994.39.2.0395>, 1994.
- 817 40. Hu, L., Liu, Y., Xiao, X., Gong, X., Zou, J., Bai, Y., Gorbarenko, S., Fahl, K., Stein, R.
818 and Shi, X.: Sedimentary records of bulk organic matter and lipid biomarkers in the
819 Bering Sea: A centennial perspective of sea-ice variability and phytoplankton
820 community, *Marine Geology*, 429, 106308,
821 <https://doi.org/10.1016/j.margeo.2020.106308>, 2020.
- 822 41. Iversen, M.H., Pakhomov, E.A., Hunt, B.P., Van der Jagt, H., Wolf-Gladrow, D. and
823 Klaas, C.: Sinkers or floaters? Contribution from salp pellets to the export flux during
824 a large bloom event in the Southern Ocean, *Deep Sea Research Part II: Topical Studies
825 in Oceanography*, 138, 116–125, <https://doi.org/10.1016/j.dsr2.2016.12.004>, 2017.
- 826 42. Iversen, M.H.: Carbon Export in the Ocean: A Biologist's Perspective, *Annual Review
827 of Marine Science*, 15, 357–381, [10.1146/annurev-marine-032122-035153](https://doi.org/10.1146/annurev-marine-032122-035153), 2023.
- 828 43. Jaramillo-Madrid, A.C., Ashworth, J., Fabris, M. and Ralph, P.J., Phytosterol
829 biosynthesis and production by diatoms (Bacillariophyceae). *Phytochemistry*, 163.46-
830 57. <https://doi.org/10.1016/j.phytochem.2019.03.018>, 2019.
- 831 44. Jaramillo-Madrid A.C., Ashworth, J., Ralph, P. J., Levels of Diatom Minor Sterols
832 Respond to Changes in Temperature and Salinity. *Journal of Marine Science and
833 Engineering*. 8(2), 85, <https://doi.org/10.3390/jmse8020085>, 2020.
- 834 45. Jansen, S.: Copepods grazing on *Coscinodiscus wailesii*: a question of size?, *Helgoland
835 Marine Research*, 62(3), 251–255, <https://doi.org/10.1007/s10152-008-0113-z>, 2008.
- 836 46. Kohlbach, D., Hop, H., Wold, A., Schmidt, K., Smik, L., Belt, S. T., Keck, Al-
837 Habahbeh, A., Woll, M, Graeve, M., Dąbrowska, A. M,s Tatarek, A., Atkinson, A., and
838 Assmy, P.: Multiple Trophic Markers Trace Dietary Carbon Sources in Barents Sea
839 Zooplankton During Late Summer. *Front. Mar. Sci.* 7:610248. doi:
840 10.3389/fmars.2020.610248, 2021.
- 841 47. Keil, R.G., Neibauer, J.A., Biladeau, C., van der Elst, K. and Devol, A.H.: A multiproxy
842 approach to understanding the "enhanced" flux of organic matter through the oxygen-
843 deficient waters of the Arabian Sea, *Biogeosciences*, 13(7), 2077–2092,
844 <https://doi.org/10.5194/bg-13-2077-2016>, 2016.
- 845 48. Kemp, A.E., Pearce, R.B., Grigorov, I., Rance, J., Lange, C.B., Quilty, P. and Salter, I.,
846 Production of giant marine diatoms and their export at oceanic frontal zones:
847 Implications for Si and C flux from stratified oceans, *Global Biogeochemical
848 Cycles*, 20(4), <https://doi.org/10.1029/2006GB002698>, 2006.
- 849 49. Krause, J.W., Schulz, I.K., Rowe, K.A., Dobbins, W., Winding, M.H., Sejr, M.K.,
850 Duarte, C.M. and Agustí, S.: Silicic acid limitation drives bloom termination and
851 potential carbon sequestration in an Arctic bloom, *Scientific Reports*, 9(1), 8149,
852 <https://doi.org/10.1038/s41598-019-44587-4>, 2019.
- 853 50. Landry, M.R., Brown, S.L., Campbell, L., Constantinou, J. and Liu, H.: Spatial patterns
854 in phytoplankton growth and microzooplankton grazing in the Arabian Sea during
855 monsoon forcing, *Deep Sea Research Part II: Topical Studies in Oceanography*, 45(10–
856 11), 2353–2368, [https://doi.org/10.1016/S0967-0645\(98\)00074-5](https://doi.org/10.1016/S0967-0645(98)00074-5), 1998.
- 857 51. Latasa, M. and Bidigare, R.R.: A comparison of phytoplankton populations of the
858 Arabian Sea during the Spring Intermonsoon and Southwest Monsoon of 1995 as
859 described by HPLC-analyzed pigments, *Deep Sea Research Part II: Topical Studies in
860 Oceanography*, 45(10-11), 2133–2170, [https://doi.org/10.1016/S0967-0645\(98\)00066-
861 6](https://doi.org/10.1016/S0967-0645(98)00066-6), 1998.
- 862 52. Le Moigne, F.A.: Pathways of organic carbon downward transport by the oceanic
863 biological carbon pump, *Frontiers in Marine Science*, 6, 634,
864 <https://doi.org/10.3389/fmars.2019.00634>, 2019.

- 865 53. Lewin, J.C.: The dissolution of silica from diatom walls, *Geochimica et Cosmochimica*
866 *Acta*, 21(3-4), 182–198, [https://doi.org/10.1016/S0016-7037\(61\)80054-9](https://doi.org/10.1016/S0016-7037(61)80054-9), 1961.
- 867 54. Liu, D., Shen, X., Di, B., Shi, Y., Keesing, J.K., Wang, Y. and Wang, Y.:
868 Palaeoecological analysis of phytoplankton regime shifts in response to coastal
869 eutrophication, *Marine Ecology Progress Series*, 475, 1–14,
870 <https://doi.org/10.3354/meps10234>, 2013.
- 871 55. Liu, T., Qiu, Y., Lin, X., Ni, X., Wang, L., Li, H. and Jing, C., Dissolved oxygen
872 recovery in the oxygen minimum zone of the Arabian Sea in recent decade as observed
873 by BGC-argo floats. *Geophysical Research Letters*, 51(12), p.e2024GL108841.
874 <https://doi.org/10.1029/2024GL108841>, 2024
- 875 56. Löder, M.G., Meunier, C., Wiltshire, K.H., Boersma, M. and Aberle, N.: The role of
876 ciliates, heterotrophic dinoflagellates and copepods in structuring spring plankton
877 communities at Helgoland Roads, North Sea, *Marine biology*, 158, 1551–1580,
878 <https://doi.org/10.1007/s00227-011-1670-2>, 2011.
- 879 57. Madhupratap, M., Kumar, S.P., Bhattathiri, P.M.A., Kumar, M.D., Raghukumar, S.,
880 Nair, K.K.C. and Ramaiah, N.: Mechanism of the biological response to winter cooling
881 in the northeastern Arabian Sea, *Nature*, 384(6609), 549–552,
882 <https://doi.org/10.1038/384549a0>, 1996.
- 883 58. Marsay, C.M., Sanders, R.J., Henson, S.A., Pabortsava, K., Achterberg, E.P. and
884 Lampitt, R.S.: Attenuation of sinking particulate organic carbon flux through the
885 mesopelagic ocean, *Proceedings of the National Academy of Sciences*, 112(4), 1089–
886 1094, <https://doi.org/10.1073/pnas.141531111>, 2015.
- 887 59. McCreary, J.P., Murtugudde, R., Vialard, J., Vinayachandran, P.N., Wiggert, J.D.,
888 Hood, R.R., Shankar, D. and Shetye, S.: Biophysical processes in the Indian
889 Ocean, *Indian Ocean biogeochemical processes and ecological variability*, 185, 9–32,
890 <https://doi.org/10.1029/2008GM000768>, 2009.
- 891 60. Mergulhao, L.P., Mohan, R., Murty, V.S.N., Guptha, M.V.S. and Sinha, D.K.:
892 Coccolithophores from the central Arabian Sea: Sediment trap results, *Journal of earth*
893 *system science*, 115, 415–428, <https://doi.org/10.1007/BF02702870>, 2006.
- 894 61. Meyers, P.A.: Organic geochemical proxies of paleoceanographic, paleolimnologic,
895 and paleoclimatic processes, *Organic geochemistry*, 27(5–6), 213–250,
896 [https://doi.org/10.1016/S0146-6380\(97\)00049-1](https://doi.org/10.1016/S0146-6380(97)00049-1), 1997.
- 897 62. Moriceau, B., Iversen, M.H., Gallinari, M., Evertsen, A.J.O., Le Goff, M., Beker, B.,
898 Boutorh, J., Corvaisier, R., Coffineau, N., Donval, A. and Giering, S.L., Copepods
899 boost the production but reduce the carbon export efficiency by diatoms, *Frontiers in*
900 *Marine Science*, 5, 82, <https://doi.org/10.3389/fmars.2018.00082>, 2018.
- 901 63. Müller, J., Wagner, A., Fahl, K., Stein, R., Prange, M. and Lohmann, G.: Towards
902 quantitative sea ice reconstructions in the northern North Atlantic: A combined
903 biomarker and numerical modelling approach, *Earth and Planetary Science Letters*,
904 306(3-4), 137–148, <https://doi.org/10.1016/j.epsl.2011.04.011>, 2011.
- 905 64. Nair, R.R., Ittekkot, V., Manganini, S.J., Ramaswamy, V., Haake, B., Degens, E.T.,
906 Desai, B.T. and Honjo, S.: Increased particle flux to the deep ocean related to
907 monsoons, *Nature*, 338(6218), 749–751, <https://doi.org/10.1038/338749a0>, 1989.
- 908 65. Nomaki, H., Rastelli, E., Ogawa, N.O., Matsui, Y., Tsuchiya, M., Manea, E.,
909 Corinaldesi, C., Hirai, M., Ohkouchi, N., Danovaro, R. and Nunoura, T.: In situ
910 experimental evidences for responses of abyssal benthic biota to shifts in phytodetritus
911 compositions linked to global climate change, *Global Change Biology*, 27(23), 6139–
912 6155, <https://doi.org/10.1111/gcb.15882>, 2021.
- 913 66. Pandey, M., Biswas, H. and Chowdhury, M.: Interlinking diatom frustule diversity
914 from the abyss of the central Arabian Sea to surface processes: physical forcing and

- 915 oxygen minimum zone, *Environmental Monitoring and Assessment*, 195(1), 161,
916 <https://doi.org/10.1007/s10661-022-10749-7>, 2023.
- 917 67. Pandey, M. and Biswas, H.: May. An account of the key diatom frustules from the
918 surface sediments of the Central and Eastern Arabian Sea and their biogeochemical
919 significance, In EGU General Assembly Conference Abstracts (EGU-131),
920 <https://doi.org/10.5194/egusphere-egu23-131>, 2023.
- 921 68. Pandey, Medhavi; Biswas, Haimanti; Birgel, Daniel; Burdanowitz, Nicole; Gaye,
922 Birgit, “Understanding biological carbon pump in the central Arabian Sea using
923 phytoplankton biomarkers and diatom frustules from surface sediments.”, Mendeley
924 Data, V1, doi: 10.17632/xm4nxzdx2.1, 2024.
- 925 69. Peng, P., Bi, R., Sachs, J.P., Shi, J., Luo, Y., Chen, W., Huh, C.A., Yu, M., Cao, Y.,
926 Wang, Y. and Cao, Z.: Phytoplankton community changes in a coastal upwelling
927 system during the last century, *Global and Planetary Change*, 224, 104101,
928 <https://doi.org/10.1016/j.gloplacha.2023.104101>, 2023.
- 929 70. Prah, F. G., Muehlhausen, L. A. and Zahnle, D. L.: Further evaluation of long-chain
930 alkenones as indicators of paleoceanographic conditions, *Geochim. Cosmochim. Acta*,
931 52(9), 2303–2310, doi:10.1016/0016-7037(88)90132-9, 1988.
- 932 71. Prah, F.G., Dymond, J. and Sparrow, M.A.: Annual biomarker record for export
933 production in the central Arabian Sea, *Deep Sea Research Part II: Topical Studies in*
934 *Oceanography*, 47(7-8), 1581–1604, [https://doi.org/10.1016/S0967-0645\(99\)00155-1](https://doi.org/10.1016/S0967-0645(99)00155-1),
935 2000.
- 936 72. Prah, F.G. and Wakeham, S.G.: Calibration of unsaturation patterns in long-chain
937 ketone compositions for palaeotemperature assessment, *Nature*, 330(6146), pp.367-
938 369, <https://doi.org/10.1038/330367a0>, 1987.
- 939 73. Prasanna Kumar S., Madhuratap, M., Kumar, M.D., Gauns, M., Muraleedharan, P.M.,
940 Sarma, V.V.S.S. and De Souza, S.N.: Physical control of primary productivity on a
941 seasonal scale in central and eastern Arabian Sea, *Journal of Earth System*
942 *Science*, 109, 433–441, <https://doi.org/10.1007/BF02708331>, 2000.
- 943 74. Prasanna Kumar. S., and Narvekar, J.: Seasonal variability of the mixed layer in the
944 central Arabian Sea and its implication on nutrients and primary productivity, *Deep Sea*
945 *Research Part II: Topical Studies in Oceanography*, 52(14-15), 1848–1861,
946 <https://doi.org/10.1016/j.dsr2.2005.06.002>, 2005.
- 947 75. Prasanna Kumar. S., Ramaiah, N., Gauns, M., Sarma, V.V.S.S., Muraleedharan, P.M.,
948 Raghukumar, S., Kumar, M.D. and Madhuratap, M.: Physical forcing of biological
949 productivity in the Northern Arabian Sea during the Northeast Monsoon, *Deep Sea*
950 *Research Part II: Topical Studies in Oceanography*, 48(6-7), 1115–1126,
951 [https://doi.org/10.1016/S0967-0645\(00\)00133-8](https://doi.org/10.1016/S0967-0645(00)00133-8), 2001.
- 952 76. Ragueneau, O., Schultes, S., Bidle, K., Claquin, P. and Moriceau, B.: Si and C
953 interactions in the world ocean: Importance of ecological processes and implications
954 for the role of diatoms in the biological pump, *Global Biogeochemical Cycles*, 20(4),
955 <https://doi.org/10.1029/2006GB002688>, 2006.
- 956 77. Rixen, T., Gaye, B. and Emeis, K.C.: The monsoon, carbon fluxes, and the organic
957 carbon pump in the northern Indian Ocean, *Progress in oceanography*, 175, 24–39,
958 <https://doi.org/10.1016/j.pocean.2019.03.001>, 2019a.
- 959 78. Rixen, T., Gaye, B., Emeis, K.C. and Ramaswamy, V.: The ballast effect of lithogenic
960 matter and its influences on the carbon fluxes in the Indian Ocean, *Biogeosciences*,
961 16(2), 485–503, <https://doi.org/10.5194/bg-16-485-2019>, 2019b.
- 962 79. Rodríguez-Miret, X., del Carmen Trapote, M., Sigró, J. and Vegas-Vilarrúbia, T.:
963 Diatom responses to warming, heavy rains and human impact in a Mediterranean lake
964 since the preindustrial period, *Science of The Total Environment*, 884, 163685,
965 <https://doi.org/10.1016/j.scitotenv.2023.163685>, 2023.

- 966 80. Roubex, V., Becquevort, S. and Lancelot, C.: Influence of bacteria and salinity on
967 diatom biogenic silica dissolution in estuarine systems, *Biogeochemistry*, 88, 47–62,
968 <https://doi.org/10.1007/s10533-008-9193-8>, 2008.
- 969 81. Roxy, M. K., Modi, A., Murtugudde, R., Valsala, V., Panickal, S., Kumar, S. P.,
970 Ravichandran, M., Vichi, M., and Levy, M.: A reduction in marine primary productivity
971 driven by rapid warming over the tropical Indian Ocean, *Geophysical Research Letters*,
972 43, 826–833, <https://doi.org/10.1002/2015GL066979>, 2016.
- 973 82. Ryderheim, F., Grønning, J. and Kiørboe, T.: Thicker shells reduce copepod grazing on
974 diatoms, *Limnology and Oceanography Letters*, 7(5), 435–442,
975 <https://doi.org/10.1002/lol2.10243>, 2022.
- 976 83. Sawant, S. and Madhupratap, M.: Seasonality and composition of phytoplankton.
977 *Current Science*, 71(11), 1996.
- 978 84. Schubert, C.J., Villanueva, J., Calvert, S.E., Cowie, G.L., Von Rad, U., Schulz, H.,
979 Berner, U. and Erlenkeuser, H.: Stable phytoplankton community structure in the
980 Arabian Sea over the past 200,000 years, *Nature*, 394(6693), 563–566,
981 <https://doi.org/10.1038/29047>, 1998.
- 982 85. Schulte, S., Mangelsdorf, K. and Rullkötter, J.: Organic matter preservation on the
983 Pakistan continental margin as revealed by biomarker geochemistry, *Organic*
984 *Geochemistry*, 31(10), 1005–1022, [https://doi.org/10.1016/S0146-6380\(00\)00108-X](https://doi.org/10.1016/S0146-6380(00)00108-X),
985 2000.
- 986 86. Schulte, S., Rostek, F., Bard, E., Rullkötter, J. and Marchal, O.: Variations of oxygen-
987 minimum and primary productivity recorded in sediments of the Arabian Sea, *Earth*
988 *and Planetary Science Letters*, 173(3), 205–221, [https://doi.org/10.1016/S0012-](https://doi.org/10.1016/S0012-821X(99)00232-0)
989 [821X\(99\)00232-0](https://doi.org/10.1016/S0012-821X(99)00232-0), 1999.
- 990 87. Sharma, S., Ha, K.-J., Yamaguchi, R., Rodgers, K. B., Timmermann, A., and Chung,
991 E.: Future Indian Ocean warming patterns, *Nature Communications*, 14, 1789,
992 <https://doi.org/10.1038/s41467-023-37435-7>, 2023
- 993 88. Silori, S., Sharma, D., Chowdhury, M., Biswas, H., Cardinal, D. and Mandeng-Yogo,
994 M.: Particulate organic matter dynamics and its isotopic signatures ($\delta^{13}\text{C}_{\text{POC}}$ and
995 $\delta^{15}\text{N}_{\text{PN}}$) in relation to physical forcing in the central Arabian Sea during SW monsoon
996 (2017–2018), *Science of the Total Environment*, 785, 147326,
997 <https://doi.org/10.1016/j.scitotenv.2021.147326>, 2021.
- 998 89. Singh, U.B. and Ahluwalia, A.S.: Microalgae: a promising tool for carbon
999 sequestration, *Mitigation and Adaptation Strategies for Global Change*, 18(1), 73–95,
1000 <https://doi.org/10.1007/s11027-012-9393-3>, 2013.
- 1001 90. Smayda, T.J. and Reynolds, C.S.: Community assembly in marine phytoplankton:
1002 application of recent models to harmful dinoflagellate blooms, *Journal of plankton*
1003 *research*, 23(5), 447–461, <https://doi.org/10.1093/plankt/23.5.447>, 2001.
- 1004 91. Smetacek, V.S.: Role of sinking in diatom life-history cycles: ecological, evolutionary
1005 and geological significance, *Marine biology*, 84, 239–251,
1006 <https://doi.org/10.1007/BF00392493>, 1985.
- 1007 92. Smith, S., Roman, M., Prusova, I., Wishner, K., Gowing, M., Codispoti, L.A., Barber,
1008 R., Marra, J. and Flagg, C.: Seasonal response of zooplankton to monsoonal reversals
1009 in the Arabian Sea, *Deep Sea Research Part II: Topical Studies in Oceanography*,
1010 45(10-11), 2369–2403, [https://doi.org/10.1016/S0967-0645\(98\)00075-7](https://doi.org/10.1016/S0967-0645(98)00075-7), 1998.
- 1011 93. Sonzogni, C., Bard, E., Rostek, F., Lafont, R., Rosell-Mele, A. and Eglinton, G.: Core-
1012 top calibration of the alkenone index vs sea surface temperature in the Indian Ocean,
1013 *Deep Sea Res. Part II Top. Stud. Oceanogr.*, 44(6), 1445–1460, doi:10.1016/S0967-
1014 0645(97)00010-6, 1997.
- 1015 94. Stoecker, D.K.: Mixotrophy among Dinoflagellates 1. *Journal of eukaryotic*
1016 *microbiology*, 46, 397–401, <https://doi.org/10.1111/j.1550-7408.1999.tb04619.x>, 1999.

- 1017 95. Stoecker, D.K., Hansen, P.J., Caron, D.A. and Mitra, A.: Mixotrophy in the marine
1018 plankton, *Annual Review of Marine Science*, 9, 311–335,
1019 <https://doi.org/10.1146/annurev-marine-010816-060617>, 2017.
- 1020 96. Swanberg, N. R., and Anderson, O.R.: The nutrition of radiolarians: Trophic activity of
1021 some solitary Spumellaria 1, *Limnology and Oceanography*, 30, 646–652,
1022 <https://doi.org/10.4319/lo.1985.30.3.0646>, 1985.
- 1023 97. Taipale, S. J., Hiltunen, M, Vuorio, K., and Peltomaa, E., Suitability of Phytosterols
1024 Alongside Fatty Acids as Chemotaxonomic Biomarkers for Phytoplankton. *Front. Plant*
1025 *Sci.* 7:212. doi: 10.3389/fpls.2016.00212, 2016.
- 1026 98. Tarran, G.A., Burkill, P.H., Edwards, E.S. and Woodward, E.M.S.: Phytoplankton
1027 community structure in the Arabian Sea during and after the SW monsoon, 1994, *Deep*
1028 *Sea Research Part II: Topical Studies in Oceanography*, 46, 655–676,
1029 [https://doi.org/10.1016/S0967-0645\(98\)00122-2](https://doi.org/10.1016/S0967-0645(98)00122-2), 1999.
- 1030 99. Ter Braak, C.J. and Smilauer, P.: CANOCO reference manual and CanoDraw for
1031 Windows user's guide: software for canonical community ordination (version 4.5),
1032 www.canoco.com, 2002.
- 1033 100. Tomas, C. R., (Ed.), *Identifying marine phytoplankton*. Elsevier, 1997.
- 1034 101. Tréguer, P., Bowler, C., Moriceau, B., Dutkiewicz, S., Gehlen, M., Aumont, O.,
1035 Bittner, L., Dugdale, R., Finkel, Z., Iudicone, D. and Jahn, O.: Influence of diatom
1036 diversity on the ocean biological carbon pump, *Nature Geoscience*, 11, 27–37,
1037 <https://doi.org/10.1038/s41561-017-0028-x>, 2018.
- 1038 102. Vallivattathillam, P., Lachkar, Z. and Lévy, M.: Shrinking of the Arabian Sea
1039 oxygen minimum zone with climate change projected with a downscaled
1040 model, *Frontiers in Marine Science*, 10, 1123739,
1041 <https://doi.org/10.3389/fmars.2023.1123739>, 2023.
- 1042 103. Véron, B., Dauguet, J. C., and Billard, C. Sterolic biomarkers in marine
1043 phytoplankton. II. Free and conjugated sterols of seven species used in mariculture.
1044 *Journal of phycology*, 34(2), 273-279. [https://doi.org/10.1046/j.1529-](https://doi.org/10.1046/j.1529-8817.1998.340273.x)
1045 [8817.1998.340273.x](https://doi.org/10.1046/j.1529-8817.1998.340273.x), 1998.
- 1046 104. Volk, T. and Hoffert, M.I.: Ocean carbon pumps: Analysis of relative strengths
1047 and efficiencies in ocean-driven atmospheric CO₂ changes, *The carbon cycle and*
1048 *atmospheric CO₂: Natural variations Archean to present*, 32, 99–110,
1049 <https://doi.org/10.1029/GM032p0099>, 1985.
- 1050 105. Volkman, J.K., Barrett, S.M., Blackburn, S.I., Mansour, M.P., Sikes, E.L. and
1051 Gelin, F.: Microalgal biomarkers: a review of recent research developments. *Organic*
1052 *Geochemistry*, 29(5-7), 1163-1179, [https://doi.org/10.1016/S0146-6380\(98\)00062-X](https://doi.org/10.1016/S0146-6380(98)00062-X),
1053 1998.
- 1054 106. Volkman, J.: Sterols in microorganisms. *Applied microbiology and*
1055 *Biotechnology*, 60, 495-506, <https://doi.org/10.1007/s00253-002-1172-8>, 2003.
- 1056 107. Wakeham, S.G., Peterson, M.L., Hedges, J.I. and Lee, C.: Lipid biomarker
1057 fluxes in the Arabian Sea, with a comparison to the equatorial Pacific Ocean. *Deep Sea*
1058 *Research Part II: Topical Studies in Oceanography*, 49, 2265–2301,
1059 [https://doi.org/10.1016/S0967-0645\(02\)00037-1](https://doi.org/10.1016/S0967-0645(02)00037-1), 2002.
- 1060 108. Ward, B.B., Devol, A.H., Rich, J.J., Chang, B.X., Bulow, S.E., Naik, H.,
1061 Pratihary, A. and Jayakumar, A.: Denitrification as the dominant nitrogen loss process
1062 in the Arabian Sea, *Nature*, 461, 78–81, <https://doi.org/10.1038/nature08276>, 2009.
- 1063 109. Wishner, K.F., Gowing, M.M. and Gelfman, C.: Mesozooplankton biomass in
1064 the upper 1000 m in the Arabian Sea: overall seasonal and geographic patterns, and
1065 relationship to oxygen gradients, *Deep Sea Research Part II: Topical Studies in*
1066 *Oceanography*, 45, 2405–2432, [https://doi.org/10.1016/S0967-0645\(98\)00078-2](https://doi.org/10.1016/S0967-0645(98)00078-2),
1067 1998.

- 1068 110. Wittenborn, A.K., Schmale, O. and Thiel, V.: Zooplankton impact on lipid
1069 biomarkers in water column vs. surface sediments of the stratified Eastern Gotland
1070 Basin (Central Baltic Sea), Plos one, 15, e0234110,
1071 <https://doi.org/10.1371/journal.pone.0234110>, 2020.
- 1072 111. Xiong, W., Mei, X., Meng, X., Chen, H. and Yang, H.: Phytoplankton
1073 biomarkers in surface sediments from Liaodong Bay and their potential as indicators of
1074 primary productivity, Marine Pollution Bulletin, 159, 111536,
1075 <https://doi.org/10.1016/j.marpolbul.2020.111536>, 2020.
- 1076 112. Zúñiga, D., Sanchez-Vidal, A., Flexas, M.D.M., Carroll, D., Rufino, M.M.,
1077 Spreen, G., Calafat, A. and Abrantes, F.: Sinking diatom assemblages as a key driver
1078 for deep carbon and silicon export in the Scotia Sea (Southern Ocean), Frontiers in
1079 Earth Science, 9, 579198, <https://doi.org/10.3389/feart.2021.579198>, 2021.

1080

1081

1082

1083

1084

1085

1086

1087

1088

1089

1090

1091

1092

1093

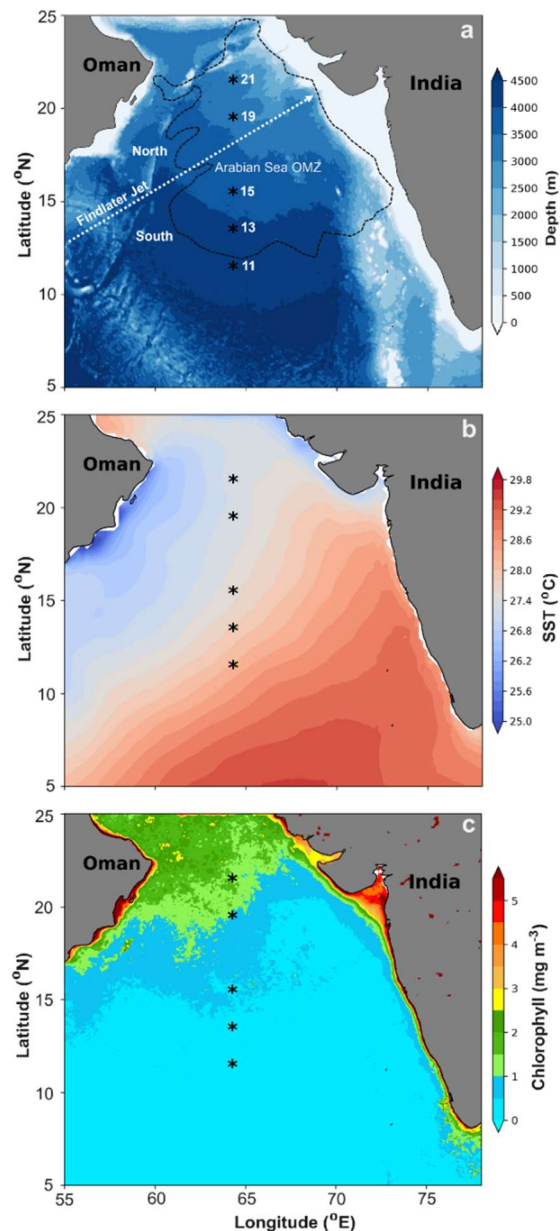
1094

1095

1096

1097

1098



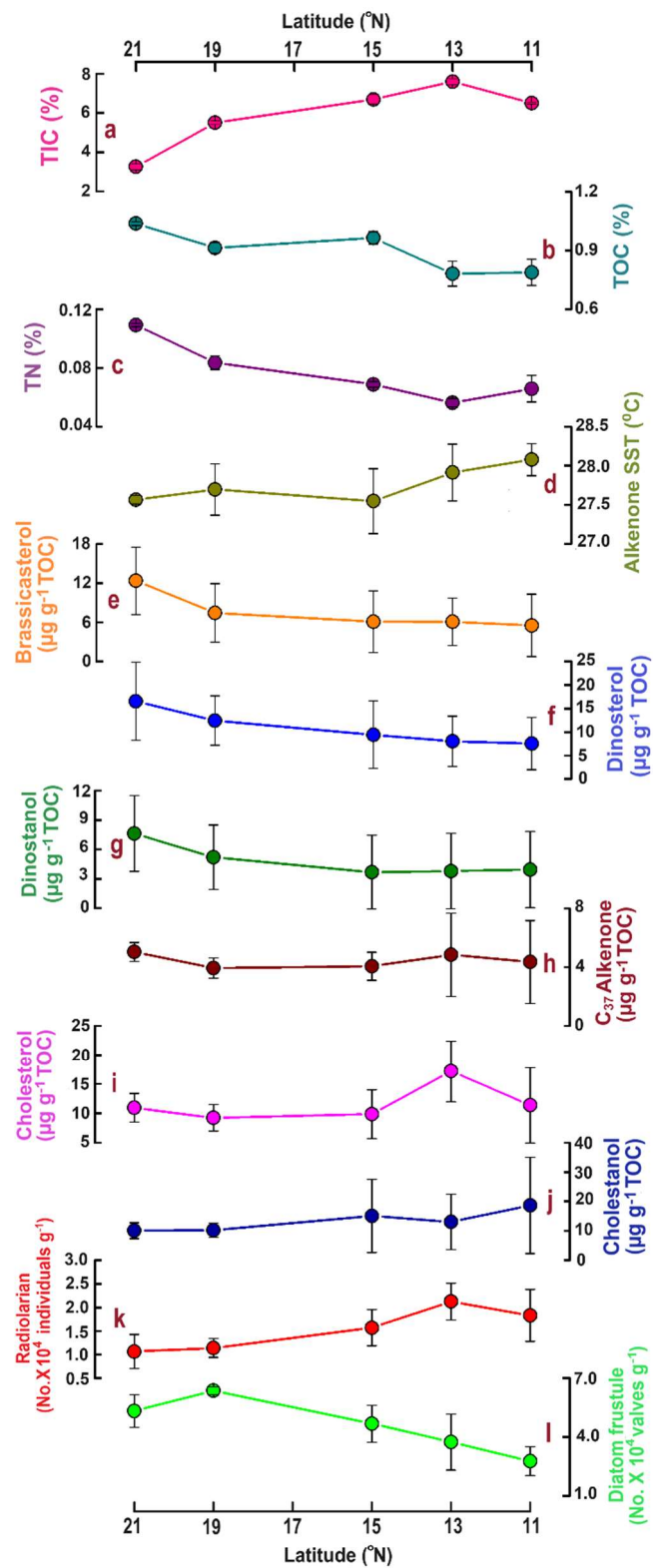
1100

1101

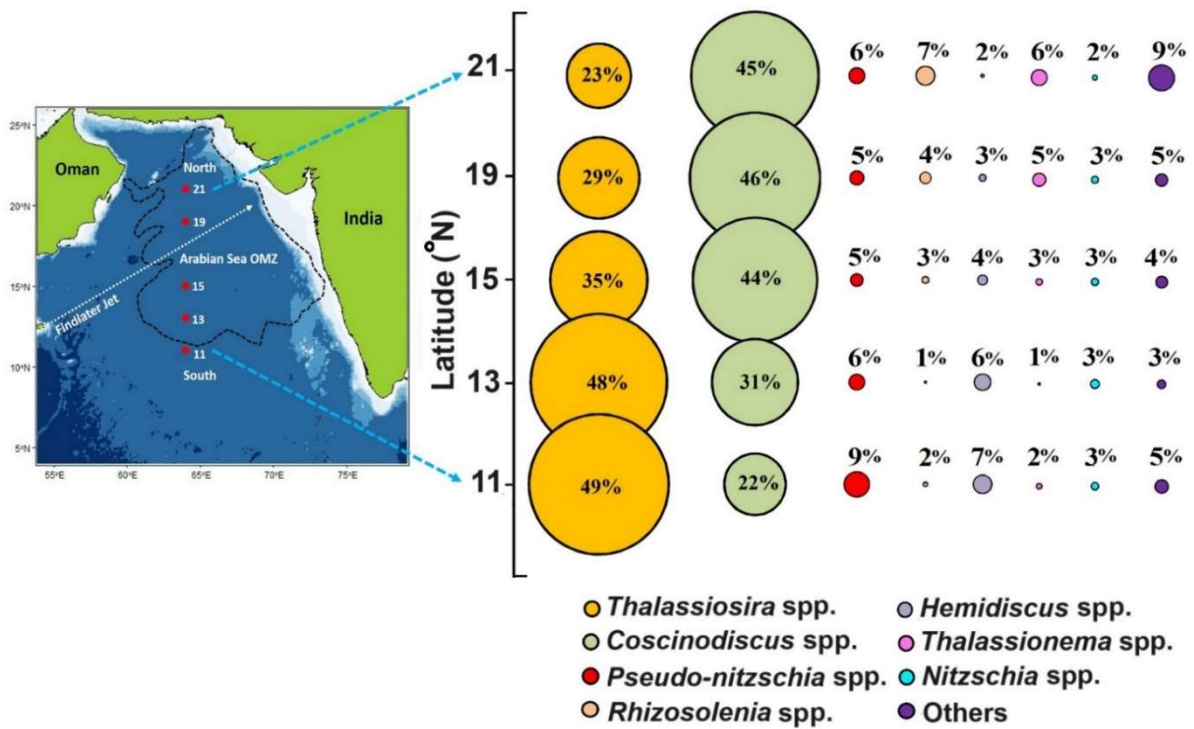
1102 **Figure 1. a)** Map showing the study locations in the Central Arabian Sea along 64° E transect
 1103 during SSD-068 (Dec 2019). The low-level atmospheric jet (Findlater Jet) is shown by a white
 1104 dashed arrow and the boundary of the Oxygen Minimum Zone (OMZ) ($0.5 \text{ mmol L}^{-1} \text{ O}_2$
 1105 concentration) is shown by a black dashed line; b) average SST (2017-2020) values depicting
 1106 spatial variability among the sampling stations from the north to south; c) average Chl *a* values
 1107 derived from the satellite for the time period 2017-2020 over the Arabian sea, indicating average
 1108 phytoplankton biomass remains higher on an annual scale for the stations in the north compared
 1109 to the south.

1110

1111
 1112
 1113
 1114
 1115
 1116
 1117
 1118
 1119
 1120
 1121
 1122
 1123
 1124
 1125
 1126
 1127
 1128
 1129
 1130
 1131
 1132
 1133
 1134
 1135
 1136
 1137
 1138



1139 **Figure 2.** The distribution of total inorganic carbon (TIC %) (a), total organic carbon (TOC %) (b), total nitrogen (TN%) (c), alkenone based sea surface temperature (SST °C) (d),
 1140 brassicasterol (e), dinosterol (f), dinostanol (g), C₃₇ alkenones (h), cholesterol (i), cholestanol (j), radiolarians (k), and diatom frustules (l) along the 64° E transect in the central Arabian Sea.
 1141
 1142



1144

1145

1146

1147 **Figure 3.** The bubble plot shows the relative percentage of diatom frustules of major species
 1148 (>3% of total abundance) from surface sediment samples (average of 0 – 0.5 cm and 0.5 - top
 1149 1 cm) along the 64° E transect in the central Arabian Sea. Individual contributions from centric
 1150 and pennate diatoms <3% were summed as “others”. The colors denote the specific
 1151 phytoplankton taxa as indicated by colored closed circle at the bottom of the panel.

1152

1153

1154

1155

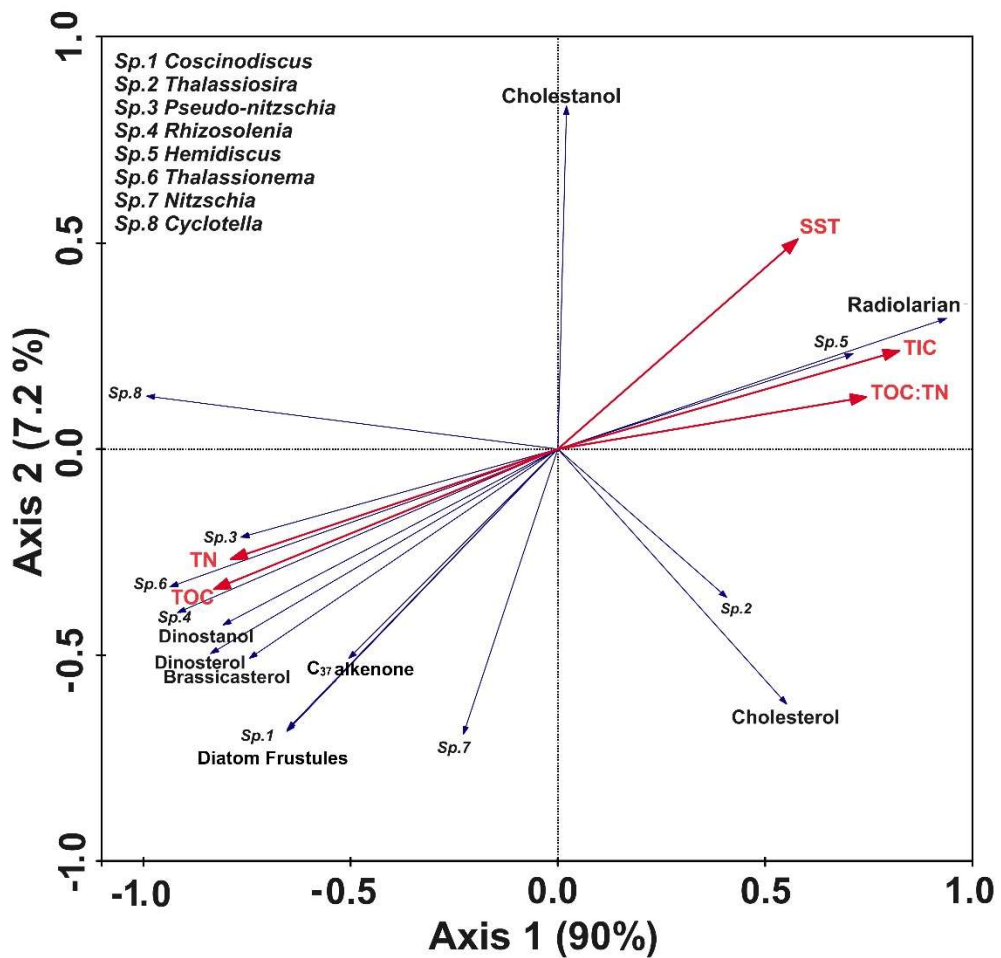
1156

1157

1158

1159

1160



1161

1162

1163 **Figure 4.** RDA biplot shows the interrelationship between the key parameters shown in blue
 1164 (diatom frustules, biomarkers, radiolarians) and bulk sedimentary parameter indicated in red
 1165 (TOC; TN, TIC, TOC:TN; SST). The names of diatoms genera are marked as “Sp.” and are
 1166 mentioned in the top left side of the panel. Axis 1 and axis 2 explained nearly 97.2% of the
 1167 variability.

1168

1169

1170

1171

1172

1173

1174

1175

1176

1177

1178

1179

1180

1181

1182

1183

1184

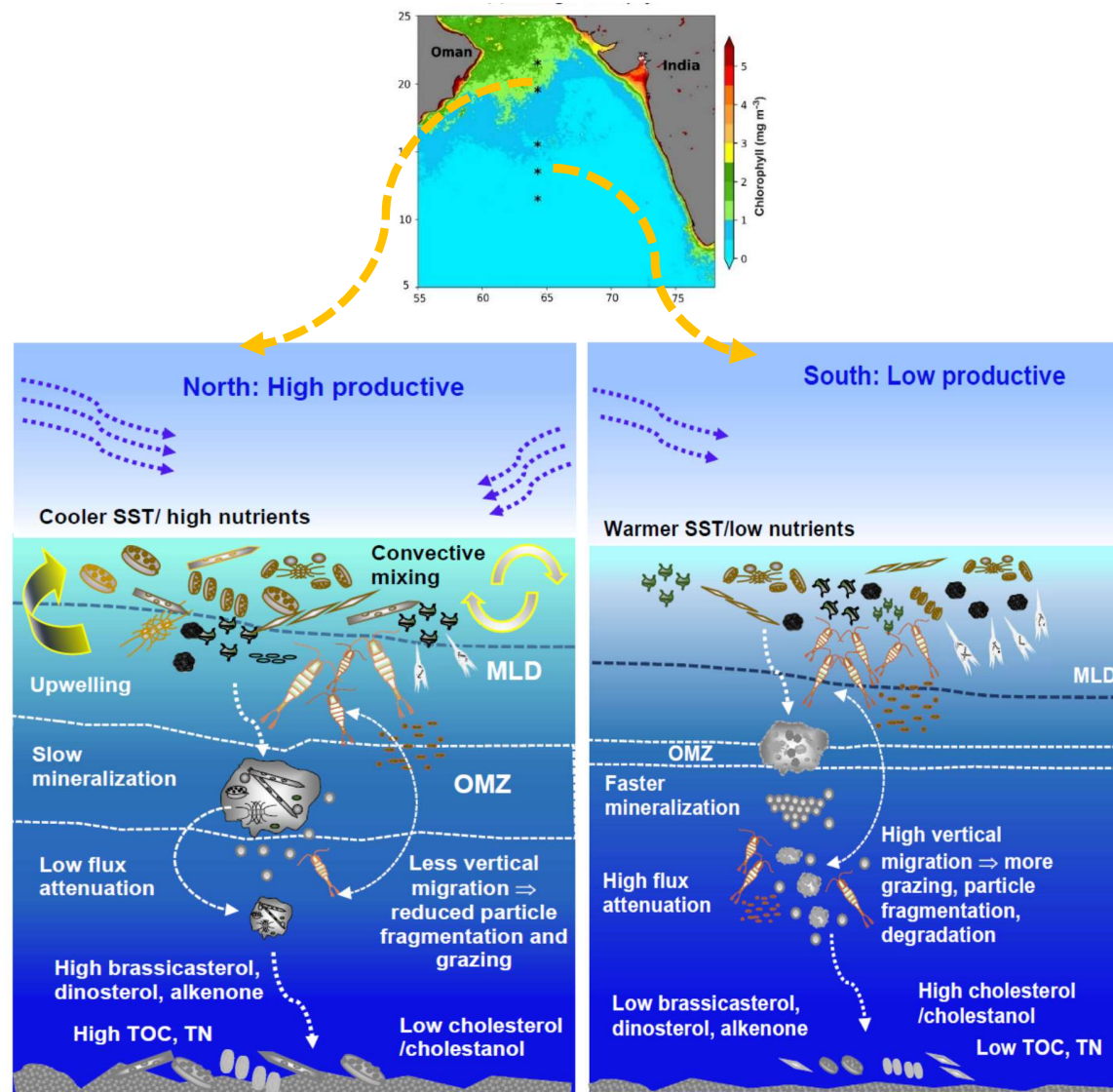
1185

1186

1187

1188

1189



1190

Figure 5. The schematic shows the spatial variability in particle flux along the 64° E transect in the central Arabian Sea.

1191 **Table 1.** Sedimentary characteristics, diatom frustules, and sterol concentrations in the surface sediments from the central Arabian Sea
 1192 (n =2±SD). The values represent the average from 0.5 and 1 cm core slices.

Latitude (°N)	21°	19°	15°	13°	11°	Average ±SD
TIC %	3.25±0.15	5.50±0.09	6.70±0.24	7.60±0.13	6.51±0.06	5.91±1.66
TOC %	1.04±0.01	0.91±0.03	0.96±0.03	0.78±0.06	0.79±0.07	0.90±0.11
TN %	0.11±0.001	0.08±0.005	0.07±0.002	0.06±0.003	0.07±0.009	0.08±0.02
TOC:TN	9.5±0.18	10.9±0.28	14±0.08	13.9±1.83	12.1±2.69	12.1±1.9
Alkenone based SST (°C)	27.6±0.05	27.7±0.33	27.5±0.42	27.9±0.36	28.1±0.20	27.8±0.2
Diatom frustule (No.×10⁴ valves g⁻¹)	5.33±0.83	6.36±0.20	4.69±0.94	3.75±1.43	2.78±0.73	4.58±1.39
Radiolarian (No.×10⁴ individuals g⁻¹)	1.07±0.36	1.14±0.20	1.57±0.38	2.13±0.39	1.83±0.55	1.54±0.45
Brassicasterol (ng g⁻¹)	128.0±52.6	68.6±43.0	58.2±43.5	46.4±24.4	42.0±33.9	68.62±34.77
Dinosterol (ng g⁻¹)	171.1±84.4	114.2±51.4	89.8±66.2	61.0±36.7	57.7±38.8	98.76±46.53
Dinostanol (ng g⁻¹)	79.0±39.4	48.0±31.5	34.7±35.2	28.3±27.8	29.8±28.0	43.95±21.05
C₃₇ alkenone (ng g⁻¹)	52.2±6.3	36.0±7.4	39.0±8.0	36.9±19.1	33.3±19.3	39.47±7.39
Cholesterol (ng g⁻¹)	113.2±24.4	84.4±23.3	94.1±36.8	132.3±29.5	87.3±42.9	102.27±20.21
Cholestanol (ng g⁻¹)	104.4±26.9	93.7±24.6	143.5±115.1	98.6±65.3	141.6±116.5	116.37±24.22
Dinosterol: Brassicasterol	1.31	1.78	1.55	1.28	1.49	1.5±0.2
Brassicasterol: Alkenone	2.41	1.82	1.41	1.25	1.16	1.6±0.5

1193

1194 **Table 2.** Average values of various parameters (n =2, ±SD) from the northern (21, 19, and 15° N) and southern stations (13 and 11° N)
 1195 of the central Arabian Sea. The values shown in **bold** “*p*” represent the level of significance (single-factor ANOVA at 95% confidence
 1196 level) between the northern and the southern stations.

1197

Parameter	North	South	<i>p</i> -value
Total Inorganic Carbon (TIC %)	5.15±1.57	7.06±0.63	0.05
Total Organic Carbon (TOC %)	0.97±0.06	0.78±0.05	0.0009
Total Nitrogen (TN %)	0.087±0.018	0.061±0.008	0.03
Alkenone derived SST (°C)	27.6±0.25	28.0±0.26	0.043
Brassicasterol (µg g⁻¹ TOC)	8.64±4.75	5.81±3.48	0.3
Dinosterol (µg g⁻¹ TOC)	12.81±6.30	7.80±4.47	0.2
Dinostanol (µg g⁻¹ TOC)	5.50±3.35	3.87±3.17	0.46
C₃₇ alkenone (µg g⁻¹ TOC)	4.34±0.81	4.60±2.33	0.8
Cholesterol (µg g⁻¹ TOC)	9.99±2.50	14.26±5.83	0.14
Cholestanol (µg g⁻¹ TOC)	11.80±6.33	15.85±11.39	0.49
Dinosterol: Brassicasterol	1.55±0.27	1.39±0.21	0.34
Brassicasterol: Alkenone	1.88±0.76	1.21±0.21	0.13
Diatom frustules (No.×10⁴ valves g⁻¹)	5.46±0.95	3.26±1.08	0.009
Radiolarian (No.×10⁴ individuals g⁻¹)	1.26±0.35	1.98±0.43	0.019

1198